



UNIVERSITA' DI NAPOLI FEDERICO II

**DOTTORATO DI RICERCA
BIOCHIMICA E BIOLOGIA MOLECOLARE E CELLULARE
XXII CICLO**

***GENERATION AND CHARACTERIZATION OF A
MOUSE MODEL FOR AEC SYNDROME***

TABLE OF CONTENTS

INTRODUCTION: Heterozygous mutations in p63 protein are causative of ectodermal dysplasia syndromes including AEC syndrome

RESULTS: Mice carrying the L514F human mutation are characterized by impairment of epidermal stemness

DISCUSSION: Our results suggest alternative hypothesis about the p63-molecular function affected by AEC mutation.

Dottoranda: Giustina Ferone
Relatore: Prof. Tommaso Russo
Prof. Caterina Missero

ANNO ACCADEMICO 2008-2009



UNIVERSITA' DI NAPOLI FEDERICO II

**DOTTORATO DI RICERCA
BIOCHIMICA E BIOLOGIA MOLECOLARE E CELLULARE
XXI CICLO**

***GENERATION AND CHARACTERIZATION OF A
MOUSE MODEL FOR AEC SYNDROME***

**Dottoranda
Giustina Ferone**

Relatore
Prof Tommaso Russo
Prof. Caterina Missero

Coordinatore
Prof. Giuseppe D'Alessio

ANNO ACCADEMICO 2008-2009

RINGRAZIAMENTI

Giunta alla conclusione di questi tre anni di dottorato sento di ringraziare tutte le persone che hanno arricchito la mia esperienza non solo scientifica ma anche e soprattutto umana. Ho avuto modo di imparare molto e per questo ringrazio la professoressa Caterina Missero che ha supervisionato il mio studio e mi ha dato l'opportunità di acquisire col tempo alcuni degli strumenti essenziali per questo lavoro nonché il metodo per avvicinarmi ai problemi scientifici. Ringrazio il professore Tommaso Russo per la costante disponibilità, per i preziosi consigli e per essere un esempio di acume e passione scientifica. Ringrazio il Prof. Giuseppe D'Alessio, coordinatore del Corso di Dottorato, che ha seguito noi dottorandi con costante impegno.

Un ringraziamento speciale va alla dottoressa Laura De Rosa, per me soprattutto un'amica, che ho avuto la fortuna di incontrare all'inizio del mio percorso e senza la quale mi è difficile immaginare di stare in laboratorio avendo creato un legame che ci ha rese complici e ha alleggerito i momenti meno belli... Ringrazio il dottor Dario Antonini per i consigli e per l'ottimismo onnipresente che in questo lavoro non guasta mai. Ringrazio tutti i dottorandi e studenti del laboratorio 1 del Ceinge con i quali ci è stato sempre un bel confronto e scambio di idee.

Non può mancare il "grazie" alla mia famiglia che ha sopportato i miei momenti di vero "sclero" in più di un'occasione e che talvolta ha ridimensionato le mie ansie e mi ha ricondotto a dare il giusto peso ad ogni cosa.

SUMMARY

AEC (*Ankyloblepharon- Ectodermal defects- Cleft lip/palate syndrome*) syndrome is an autosomal dominant disorder mainly characterized by ectodermal dysplasia, skin erosions and cleft lip and/or palate. This disorder is caused by missense mutation in the Sterile Alpha Motif (SAM) domain of the transcription factor p63, a crucial regulator of embryonic development of stratified epithelia.

To fully understand the molecular mechanisms associated with the pathogenesis of AEC syndrome, we have generated and characterized a mouse model carrying the clinically relevant L514F human mutation. $p63^{+/L514F}$ mice showed a lethal phenotype due to a severe cleft of the secondary palate. Skin was hypoplastic and fragile recapitulating at least in part the phenotype observed in AEC patients.

Gene expression analysis performed on epidermis isolated from $p63^{+/L514F}$ versus wild type mice, showed that only a subset of *bona-fide* direct targets of p63 were affected by the mutation at least in heterozygosity.

To further understand the effect of the mutation on the p63 protein function, we crossed our chimeras carrying L514F in the germ line cells and $p63^{+/-}$ and we obtained $p63^{-/L514F}$ mice. In the absence of the wild-type allele, $p63^{-/L514F}$ mice display a comparable phenotype to that of $p63^{-/-}$ mice suggesting that mutations in the SAM domain severely affect the entire function of p63 α protein.

Although p63 has an important role in proliferation and differentiation of epidermis, we demonstrated that these two processes occurred properly in $p63^{+/L514F}$. In contrast, we collected strong evidence in line with an

impairment of the proliferative potential and/or survival of mutant epidermal stem cells. Flow cytometric analysis with stem cell surface markers, indicated a strong reduction in the stem cell population of mutant mice compared to wild-type. In addition, clonogenic analysis performed on keratinocytes obtained from $p63^{+/L514F}$ and wild-type epidermis, showed a decrease of size and number of mutant colonies. Finally, $p63^{+/L514F}$ epidermis displayed low protein and mRNA levels of the skin progenitor cell marker Krt15 (Keratin 15).

Furthermore, we found increased apoptosis in the basal layer of epidermis, where stem cells are putatively located. This finding suggested that the defect in epidermal stem cell compartment could be associated to a defect in cell survival. In conclusion, our mouse model will be useful to understand the pathogenesis of this complex disorder and to characterized more in details the identity and properties of epidermal stem cells.

SOMMARIO

La sindrome AEC (*Ankyloblepharon- Ectodermal defects- Cleft lip/palate syndrome*) è una malattia autosomica dominante caratterizzata da dispasia ectodermica, erosioni cutanee e labioschisi e/o palatoschisi. Questo disordine è causato da mutazioni missenso nel dominio Sterile Alpha Motif (SAM) del fattore di trascrizione p63, un regolatore cruciale nello sviluppo embrionale degli epiteli stratificati.

Per comprendere a pieno i meccanismi molecolari associati alla patogenesi della sindrome AEC, abbiamo generato e caratterizzato un modello murino della mutazione umana L514F, rilevante dal punto di vista clinico. I topi $p63^{+/L514F}$ mostrano un fenotipo letale dovuto a grave schisi del palato secondario. La cute è ipoplastica e fragile ricapitolando almeno in parte il fenotipo osservato nei pazienti.

L'analisi di espressione genica effettuata su epidermide isolata da topi $p63^{+/L514F}$ e wild-type, ha mostrato che solo un sotto-gruppo di di *bona-fide* target diretti di p63 è alterata in presenza della mutazione, almeno in eterozigosi.

Per comprendere ulteriormente l'effetto della mutazione sulle funzioni della proteina p63, abbiamo incrociato le chimere con la mutazione L514F in cellule della linea germinale con topi $p63^{+/-}$ per ottenere topi $p63^{-/L514F}$.

In assenza dell'allele wild-type, i topi $p63^{-/L514F}$ mostrano un fenotipo comparabile a quello dei topi $p63^{-/-}$ suggerendo che la mutazione nel dominio SAM altera severamente l'intera funzione della proteina p63 α .

Sebbene p63 abbia un ruolo importante nella proliferazione e nel differenziamento dell'epidermide, abbiamo dimostrato che questi due

processi avvengono correttamente nei topi $p63^{+/L514F}$. In contrasto, abbiamo collezionato una serie di forte evidenze in linea con un indebolimento nel potenziale proliferativo e/o nella sopravvivenza delle cellule staminali dell'epidermide. L'analisi citofluorimetrica con marker di superficie delle cellule staminali dell'epidermide, ha indicato una forte riduzione nella popolazione di cellule staminali nei topi mutanti rispetto ai wild-type. Inoltre, analisi clonogeniche effettuate su cheratinociti ottenuti da epidermide di topi $p63^{+/L514F}$ e wild-type, hanno mostrato una diminuzione delle colonie mutanti, sia in numero che in dimensioni. In fine l'epidermide dei topi $p63^{+/L514F}$ è caratterizzata da una riduzione dei livelli proteici e del mRNA di Krt15 (cheratina 15), un marker delle cellule progenitrici cutanee.

Inoltre, abbiamo trovato un aumento di apoptosi nel compartimento basale dell'epidermide, sede delle cellule staminali. Questo risultato ci ha suggerito che il difetto nella popolazione di cellule staminali dell'epidermide potrebbe essere associato ad un difetto nella sopravvivenza cellulare.

In conclusione, il nostro modello murino sarà utile per capire le basi patogenetiche di questo complesso disordine e per caratterizzare più nel dettaglio l'identità e le proprietà delle cellule staminali dell'epidermide.

INDEX

1. INTRODUCTION

1.1 Epidermis.....	pag. 1
1.2 Stem cells of epidermis.....	pag. 3
1.3 Structure and function of p63 protein.....	pag. 5
1.4 Phenotype of p63-deficient mice.....	pag. 7
1.5 p63-Associated disorders.....	pag. 11
1.6 AEC syndrome.....	pag. 13
1.7 The Sterile alpha motif (SAM) domain.....	pag. 14

2. MATERIALS AND METHODS

2.1 Targeting vector.....	pag. 17
2.2 Growing E14Tg2A ES cells.....	pag. 19
2.3 Gene Targeting in Embryonic Stem (ES) Cells and Generation of p63 ^{+/L514F} mice.....	pag. 19
2.4 Southern blotting analysis.....	pag. 21
2.5 Mouse genotyping.....	pag. 22
2.6 Histopathology and Immunostaining.....	pag. 23
2.7 Western Blot.....	pag. 24
2.8 BrdU incorporation assay.....	pag. 25
2.9 Skin Barrier Assays.....	pag. 25
2.10 Primary keratinocytes.....	pag. 26
2.11 Colony-forming assays.....	pag. 26
2.12 Real-time RT-PCR.....	pag. 27
2.13 Fluorescent activated cell sorting (FACS) analysis.....	pag. 27

2.14 Gene expression microarrays.....pag. 27

3. RESULTS

3.1 Generation of a mouse model carrying the L514F AEC human-mutation.....pag. 29

3.2 p63^{+L514F} mice recapitulate the phenotype of AEC patients.....pag. 31

3.3 Global gene expression profile of p63^{+L514F}.....pag. 37

3.4 Epidermal proliferation and differentiation are not affected in p63^{+L514F} mice.....pag. 39

3.5 Defective proliferative potential of epidermal stem cells in AEC syndrome.....pag. 44

 3.5.1 Colony-forming assay.....pag. 44

 3.5.2 FACS analysis to define progenitor cell population..... pag. 46

 3.5.3 Expression of the skin stem cell marker Krt15..... pag. 47

3.6 Skin hypoplasia is caused by increased apoptosis of basal cell compartmentpag. 50

3.7 Loss or gain of function? Analysis of mutation in p63^{-L514F} mice.....pag. 51

3.8 Molecular pathways involved in the pathogenesis of AEC syndrome.....pag. 53

4. DISCUSSION.....pag. 59

INDEX OF FIGURES

Figure 1. The skin and its appendages.....	pag. 2
Figure 2. Schematic illustration of ΔN and TA p63 isoforms.....	pag. 5
Figure 3. Phenotype of p63 ^{-/-} mice.....	pag. 8
Figure 4. Critical stages of palate development.....	pag. 9
Figure 5. Genotype to phenotype correlation of p63 mutations.....	pag. 12
Figure 6. Position of missense mutations in the p63 SAM domain that cause AEC syndrome.....	pag. 16
Figure 7. Generation of the p63 ^{+/L514F} knock-in mouse model.....	pag. 30
Figure 8. Cleft palate of p63 ^{+/L514F} mice.....	pag. 31
Figure 9. Mutant palatal shelves do not come in contact.....	pag. 32-33
Figure 10. Skin hypoplasia and fragility in p63 ^{+/L514F} mice.....	pag. 34
Figure 11. Expression of Krt6 on epidermis of wild-type and p63 ^{+/L514F} newborn mice.....	pag. 35-36
Figure 12. Global gene expression profile of p63 ^{+/L514F}	pag. 38
Figure 13. Cell proliferation is unaffected in p63 ^{+/L514F} skin.....	pag. 40
Figure 14. Epidermal differentiation of p63 ^{+/L514F} mice.....	pag. 41-42
Figure 15. Phenotype of p63 ^{+/L514F} at E16.5.....	pag. 43
Figure 16. Colony-forming assay.....	pag. 45
Figure 17. Epidermal stem cells from epidermis of newborn mice.....	pag. 47
Figure 18. Krt15 is reduced in p63 ^{+/L514F} newborn skin at both mRNA and protein levels.....	pag. 48
Figure 19. Krt15 is expressed at low levels in AEC patients.....	pag. 49
Figure 20. Caspase 3 is increased in the epidermis of p63 ^{+/L514F} mice.....	pag. 50

Figure 21. Comparison between p63^{-/L514F} and p63^{-/-} mice.....pag. 52

Figure 22. Expression of Fgfr2 isoforms in p63^{+/L514F} mice.....pag. 54

Figure 22. A. Levels of ERK phosphorylation in p63^{+/L514F} and wild-type keratinocytes.....pag. 55

Figure 23. Expression of Igf2 in p63^{+/L6514F} mice epidermis.....pag. 56

Figure 22. Levels of Akt phosphorylation in p63^{+/L514F} in p63^{+/L514F} and wild-type keratinocytes.....pag. 57

ABBREVIATIONS

αTUB	α Tubulin
AEC syndrome	Ankyloblepharon- Ectodermal defects- Cleft lip/palate syndrome
BAC	Bacterial artificial chromosome
BrdU	5-bromo-2-deoxyuridine
Bmp4	Bone morphogenetic protein 4
Cdh1	E-cadherin
EEC syndrome	Ectrodactyly- Ectodermal dysplasia- Cleft lip/palate syndrome
ED	Ectodermal dysplasia
EPU	Epidermal proliferative unit
ES cells	Embryonic stem cells
FACS	Fluorescent activated cell sorting
FDR	False Discovery Rate
Fgf8	Fibroblast growth factor 8
Fgfr2	Fibroblast growth factor receptor 2
Igfr1	Insulin growth factor receptor 1
Igf2	Insulin growth factor 2
Ivl	Involucrin
Lor	Loricrin
H&E	Haematoxylin and Eosin
MEE	Medial edge epithelial
Krt1	Keratin 1
Krt2	Keratin 2
Krt5	Keratin 5
Krt6	Keratin 6
Krt8	Keratin 8
Krt10	Keratin 10
Krt15	Keratin 15
Krt14	Keratin 14
Krt79	Keratin 79

O/n	Overnight
PCR	Polymerase chain reaction
PBS	Phosphate-buffered saline
PFA	Paraformaldehyde
RHS syndrome	Rapp-Hodgkin syndrome
R.t.	Room temperature
SAM	Sterile Alpha Motif
Shh	Sonic hedgehog
TA cells	Transit amplifying cells
Y2H	Yeast two-hybrid

1. INTRODUCTION

1.1 Epidermis

The epidermis is the outermost layer of the skin, composed of a stratified squamous epithelium that rests on top of a basement membrane, rich in extracellular matrix, which separates it and its appendages, including the hair follicles and sweat glands, from the underlying mesenchymally derived dermis. The epidermis and its appendages provide a protective barrier that keeps microbes out and essential body fluids in and are able to withstand the physical and chemical traumas.

The epidermis is composed of 4-5 layers depending on the region of skin being considered. Those layers in descending order are the cornified layer (stratum corneum), granular layer, spinous layer and basal layer (Fig.1). The stratified squamous epithelium is maintained by cell division within the basal layer. Differentiating cells slowly displace outwards through the spinous layer to the stratum corneum, where anucleate corneal cells are continuously shed from the surface (desquamation). In normal skin the rate of production equals the rate of loss, taking about two weeks for a cell to migrate from the basal cell layer to the top of the granular cell layer, and an additional two weeks to cross the stratum corneum (1).

Introduzione

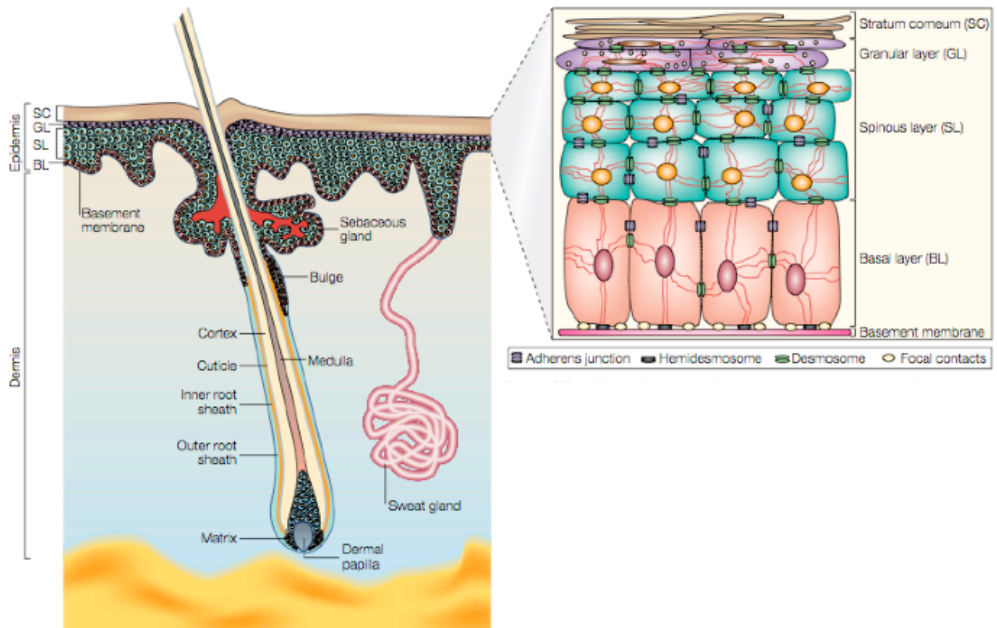


Figure 1. The skin and its appendages. Mammalian skin consists of the epidermis and dermis, separated by a basement membrane. The epidermis is a stratified squamous epithelium composed by: the basal layer (BL), on top of the basement membrane consisting of proliferating, transit-amplifying cells (TA) interspersed to epidermal stem cells; spinous layer (SL), granular layer (GL) and the stratum corneum (SC). Also shown is a cross-section of a hair follicle: progenitors of hair follicle reside in the portion indicated as bulge. (Adapted from Fuchs, *Getting under the skin of epidermal morphogenesis*, Nat Rev Genet, 2002).

1.2 Stem cells of epidermis

The epidermis undergoes continual self-renewal to repair damaged tissue and replace old cells. To continuously renewing, skin depends on stem cells, which reside in the adult hair follicle, sebaceous gland and epidermis for the purpose of maintaining tissue homeostasis, regenerating hair and repairing the epidermis after injury.

Epidermal stem cells do not possess a precise niche but are located in the basal layer of epidermis interspersed with cells committed to differentiation and are thought to proliferate at a slow rate (2). Epidermal stem cells give rise to a cell population with a reduced proliferative potential, named transit-amplifying (TA) cells. After a limited number of divisions, TA cells give rise to committed cells that differentiate suprabasally in mature keratinocytes (3). Morphological and kinetics studies showed that dorsal mouse skin is organized in “epidermal proliferative units” (EPU) each consisting of a group of cells containing proliferative and functioning elements. The proliferative elements are located in the basal layer and are constituted by a stem cell and its progeny while the differentiated cells are positioned in a column (one cell wide) above the proliferative cell group (4). More recently another model to explain the homeostasis of epidermis has been proposed. This model is based on the assumption that a single type of progenitor cell maintains the epidermis. In this study, the authors posit that all proliferative cells in the basal layer might be functionally equivalent, such that epidermal progenitor cells give rise directly to committed spinous cells without entering a TA phase (5). Thus, the identity of stem cells in the epidermis remains to be fully established.

It was been reported that epidermal stem cells can be distinguished from

other basal cells by using two markers. Immunofluorescence studies showed that putative stem cells expressed high levels of α_6 (also named CD49f) and β_1 integrins and, in addition, low levels of transferrin receptor (also named CD71) (6, 7).

However, most of the genes that are associated with skin epithelial stem cells are also expressed, although at lower level, in the transit-amplifying cells, which raises the question of whether these markers function to maintain stem-cell character or proliferative capacity. An example of this is p63, a p53 homologue that is expressed throughout the basal layer of the epidermis. Mutations in p63 gene are causative of several syndromes including the AEC syndrome that is object of this project.

1.3 Structure and function of p63 protein

The p63 gene is a homologue of the archetypal tumor suppressor gene p53 (8-12). It consists of 16 exons located on chromosome 3q28. At least six different protein isoforms can be produced, due to two different promoter sites and three different splicing routes. The amino-terminal ends are called TA and ΔN , and at the carboxy-terminal end, α , β and γ termini can be synthesized (Fig.2). Several functional domains have been identified. The central DNA-binding domain and isomerization domain are present in all p63 isoforms. The canonical transcription activation (TA) domain is located at the amino-terminal end of the TAp63 isoforms. The ΔN -isoforms also contain an amino-terminal transactivation domain (13, 14). The carboxy-terminal end has two additional domains: the sterile-alpha-motif (SAM) domain and a transactivation inhibitory (TI) domain, which are both only present in the largest carboxy-terminal p63 α variant (Fig.2) (15).



Figure 2. Schematic illustration of ΔN and TA p63 isoforms. Exons are represented by rectangles encoding the transactivation domain (blue), the DNA binding domain (red), the oligomerization domain (green) and the sterile α motif (light grey) followed by the transactivation inhibitory domain

Introduzione

(encoded by the C-terminal part of exon 14) (Adapted from Keyes et al, *p63 heterozygous mutant mice are not prone to spontaneous or chemically induced tumors*, PNAS, 2006)

p63, p53 and the third member p73, constitute a family of key transcriptional regulators in cell growth, differentiation and apoptosis. While p53 is a major player in tumorigenesis (16), p63 and p73 appear to have pivotal roles in embryonic development (17-19).

More in detail, p63 has a crucial role in embryonic development of stratified epithelia. The more abundant isoform $\Delta Np63\alpha$ is expressed from cells of the basal layer of epidermis (12).

1.4 Phenotype of p63-deficient mice

Mice lacking all p63 isoforms shed light on the crucial role of p63 in the development of ectodermal derived tissues; indeed p63^{-/-} mice die at birth and show severe developmental abnormalities, including limb truncations, and defects in the epidermis and its appendages (17, 18). The surface epithelium is thin, lacks stratification, and does not express markers of epithelial differentiation. Ectodermal organs such as hairs, whiskers, teeth and several glands, including mammary, salivary and lacrimal glands, are lacking (Fig. 3A-B). The epithelial phenotype has been interpreted to result from either lack of commitment of the immature ectoderm to epidermal lineages (17), or lack of proliferative potential of the p63-deficient epidermal stem cells (18) (Fig. 3C).

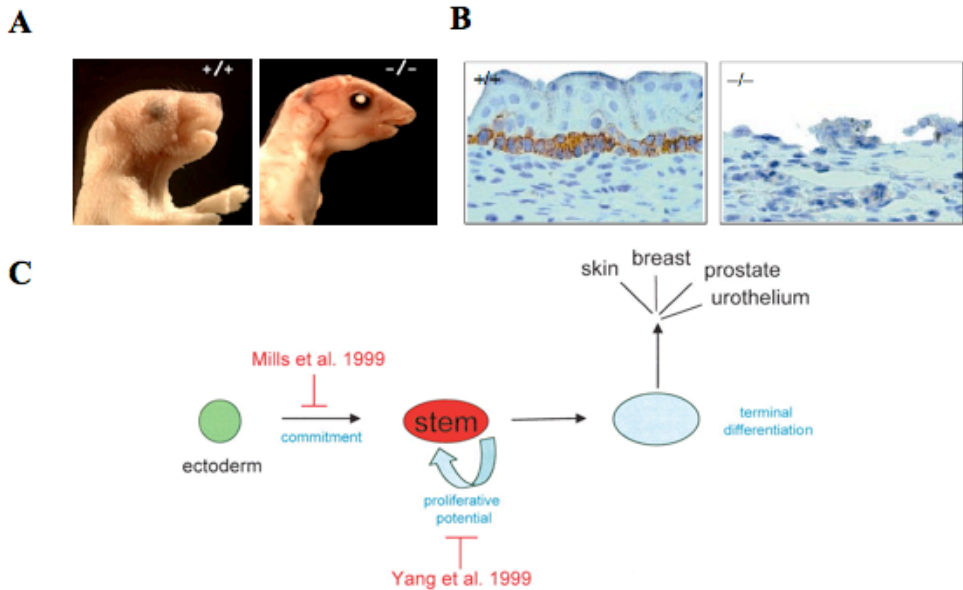


Figure 3. Phenotype of $p63^{-/-}$ mice. **A.** $p63$ mice on postnatal day1 (P1) have hypoplastic upper and lower jaws, and have no eyelids, whisker pads, skin and related appendages, which are present on the wild-type control. **B.** Anti-keratin 5 antibody staining in epidermis of $p63^{-/-}$ and control littermates. **C.** Deduction of $p63$ function in epithelial morphogenesis. The steps where the process of epidermal development is blocked in $p63^{-/-}$, were deduced separately by Mills et al. (1999) and Yang et al. (1999) as commitment and proliferative potential of stem cells, respectively (Fig. A and B adapted from Yang et al, *p63 is essential for regenerative proliferation in limb, craniofacial and epithelial development*, Nature, 1999)

These observations suggest that $p63$ has a crucial role in tissue morphogenesis and maintenance of epithelial stem cell compartment. Among other defects, $p63^{-/-}$ mice display cleft lip and palate. In wild-type mice, the palatal shelves first appear at around E12.5 and rapidly grow in a

vertical plane flanking the developing tongue (Fig. 4). During E12.5–E13.5, the shelves, consisting of rapidly proliferating mesenchymal cells, undergo elevation to bring them into horizontal apposition above the tongue. Following elevation, the medial edge epithelial (MEE) of the opposing palatal shelves fuse in the midline through interactions of cell adhesion molecules and desmosomes. The resulting epithelial seam is rapidly removed through a combination of programmed cell death, epithelial cell migration and transdifferentiation (20, 21). Palatogenesis is considered to be complete in mouse by around E15.5 (Fig. 4).

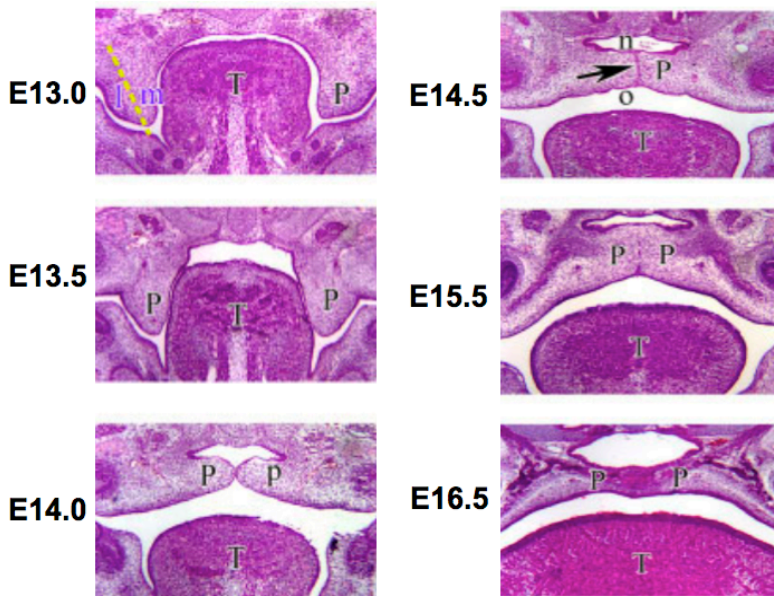


Figure 4. Critical stages of palate development. Mouse palatogenesis starts at embryonic day (E) 11.5. By E13.5, palatal shelves (P) are on both sides of the tongue (T). Between E13.5 and E14.0, palatal shelves turn horizontally above the tongue and face each other along the midline. At E14.5, palatal fusion begins to take place. The arrow indicates the midline

epithelial seam. n, nasal epithelium; o, oral epithelium. From E15.5 to E16.5, palatal fusion is completed throughout the entire palate (Adapted from Chai, Y, *Recent advances in craniofacial morphogenesis*, Dev Dyn, 2006).

In $p63^{-/-}$ mice, an abnormal morphogenesis of the medial and lateral nasal and maxillary processes is present at E10.5. Analysis of key signaling molecules revealed that these defects result from increased Bmp4 signaling in the epithelium of the facial processes (22). In addition, defective proliferation of mesenchymal cells of the maxillary processes at E11.5 resulted in absence of the anterior region of the palatal shelves and, subsequently, cleft palate. Cleft lip is caused by down-regulation of the key signaling molecules Fibroblast growth factor 8 (Fgf8) and Sonic hedgehog (Shh) that led to reduced mesenchymal cell proliferation, regional growth defects and altered morphogenesis of the nasal processes (22).

1.5 p63-Associated disorders

Heterozygous mutations in the human p63 gene cause developmental disorders, characterized by various combinations of ectodermal dysplasia (ED), limb malformations and orofacial clefting (23, 24). To date, seven different disorders have been linked to mutations in the p63 gene (25). These conditions have overlapping phenotypic features, but some genotype-phenotype correlations have emerged (26). EEC syndrome (Ectrodactyly Ectodermal dysplasia and Cleft lip/palate, OMIM 604292) is the most common p63-linked ED. It is characterized by three major clinical symptoms: cleft lip and/or palate, ED (abnormal teeth, skin, hair, nails and sweat glands) and limb malformations in the form of split hand/foot (ectrodactyly) and/or fusion of fingers/toes (syndactyly). About 10% of p63-linked patients have AEC (Ankyloblepharon Ectodermal defects Cleft lip/palate) syndrome (OMIM 106260). AEC syndrome is characterized by ED and orofacial clefting, but does not show the severe limb malformations seen in EEC syndrome. EEC and AEC syndromes are good examples of a strong genotype – phenotype association (Fig. 5). Mutations in EEC syndrome are clustered in the DNA binding domain, and most likely alter the DNA-binding properties of the protein. In contrast, mutations in AEC syndrome are clustered mostly in the SAM and rarely in TI domains in the carboxy-terminus of p63 α (27, 28). The SAM domain is involved in protein-protein interactions, whereas the TI domain can bind intramolecularly to the transactivation domain, thereby inhibiting transcription activation (15). The other p63-associated syndromes are: Limb Mammary Syndrome (LMS, OMIM 603543), Acro-Dermato-Ungual-Lacrimal-Tooth

syndrome (ADULT, 103285) and non-syndromic Split Hand/Foot Malformation (SHFM4, OMIM 605289) (29). All p63-linked disorders are inherited in an autosomal dominant manner and mutations are thought to have either dominant-negative or gain-of-function effects (30).

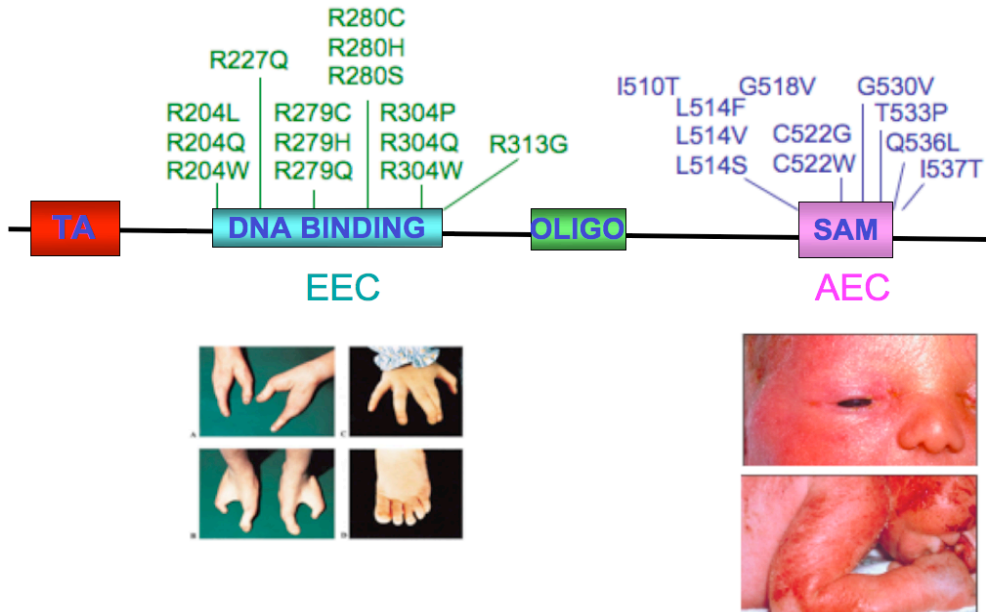


Figure 5. Genotype to phenotype correlation of p63 mutations. Mutations in EEC syndrome are clustered in the DNA binding domain (green) and are strongly characterized by limb malformations in the form of split hand/foot (ectrodactyly) and/or fusion of fingers/toes (syndactyly) (Left image, adapted from Celli et al, *Heterozygous germline mutations in the p53 homolog p63 are the cause of EEC syndrome*, Cell, 1999); in contrast, mutations in AEC syndrome are clustered in SAM domain (blue) and fulfill the criteria of ectodermal dysplasia and orofacial clefting (Right image, adapted from McGrath et al, *Hay-Wells syndrome is caused by heterozygous missense mutations in the SAM domain of p63*, Hum Mol Genet, 2001).

1.6 AEC syndrome

Ankyloblepharon-Ectodermal defects Cleft lip/palate syndrome (AEC), also known as Hay–Wells syndrome, was first reported by Hay and Wells in 1976 (31). Its main symptoms are ankyloblepharon (fusion of the eyelids), ectodermal defects and cleft lip and palate. Clinical manifestations have different penetrance: about 75% of patients have severe skin erosions at birth, with some AEC patients reported to have up to 70% denuded skin (32). By 4 – 5 years age erosions could disappear, except for the head and auricular region. Alopecia is also often linked to AEC syndrome as are absence of eyelashes and eyebrows. Clefting occurs approximately in 80% of AEC patients. The denominative ankyloblepharon occurs only in 44% of AEC cases. Hearing loss has been reported in about 40% of the patients. AEC patients have nail and teeth defects in about 75–80% of cases. About half of the patients have lacrimal duct atresia. One significant difference to the other p63 syndromes is the absence of limb malformations; only a few number of patients have a mild syndactyly (29). AEC syndrome is very similar to Rapp Hodgkin syndrome (RHS, OMIM 129400); these syndromes are possibly variable manifestations of the same clinical entity (25, 27). Although AEC and RHS syndromes have always been linked to the α -tail of the p63 gene, three novel mutations were recently discovered in the 5' end of the p63 gene (33).

1.7 The Sterile alpha motif (SAM) domain

Determining the state of protein complex formation is critical for understanding many signaling and structural pathways. Often protein interactions are mediated through conserved domains. The SAM domain is a commonly occurring motif, facilitating diverse interactions including protein homo-dimerization, hetero-dimerization, and even RNA binding (34, 35). Defects in the SAM domains of proteins have been observed in a number of human diseases (35, 36). Although in vitro SAM domains are capable of forming both homo- and hetero-oligomers, it remains unclear how SAM domains mediate protein interactions under in vivo settings, where most proteins are expressed at levels much lower than those often used in biochemical and structural analyses. It is also unknown how these domains might be engaged in hetero or homo-oligomer formation in vivo, in the presence of the full-length proteins expressed at their endogenous levels and in the presence of additional interacting partners.

The full-length α -isoform of p63 and p73 contains at the C-terminal a SAM module, which is absent in all other isoforms. These isoforms show p53-like function dramatically reduced in comparison with other non-SAM-containing isoforms, suggesting that SAM domain could be responsible for those functional differences (37). The SAM domain consists of a small (~70-amino acid) protein-protein interaction module found in a variety of proteins involved in developmental regulation, signal transduction and transcription (38). The common mechanism of interaction is homo- and hetero-oligomerization among similar SAM domains (39, 40). The solution structure of the C-terminal domain of human p63 (505-579) was solved through NMR spectroscopy (41). The resulting structure shows the

characteristic five-helix bundle topology observed in other SAM domains (38). It includes helix 1 ($\alpha 1$; residues 514–521), helix 2 ($\alpha 2$; residues 527–533), a short 3^{10} helix (H3; residues 538–542), helix 4 ($\alpha 4$; residues 546–551), and helix 5 ($\alpha 5$; residues 556–573). The five helices are tightly packed together via an extended hydrophobic core and form a globular and compact structure (Fig. 6). Possibly, the unknown interacting protein is involved in the selection of specific p63 target genes. Such a role would be in accordance with the specific phenotype of AEC syndrome, which in contrast to EEC syndrome, does not include ectrodactyly, but instead presents with ankyloblepharon and severe scalp dermatitis (28).

Interestingly, none of the residues that are involved in dimerization or oligomerization in crystal structures of other SAM domains has been found to be mutated in p63. This observation could suggest that the SAM domain of p63 is capable of interaction with a non-SAM domain protein. Disruption of this interaction then gives rise to the typical developmental defects of AEC syndrome (28).

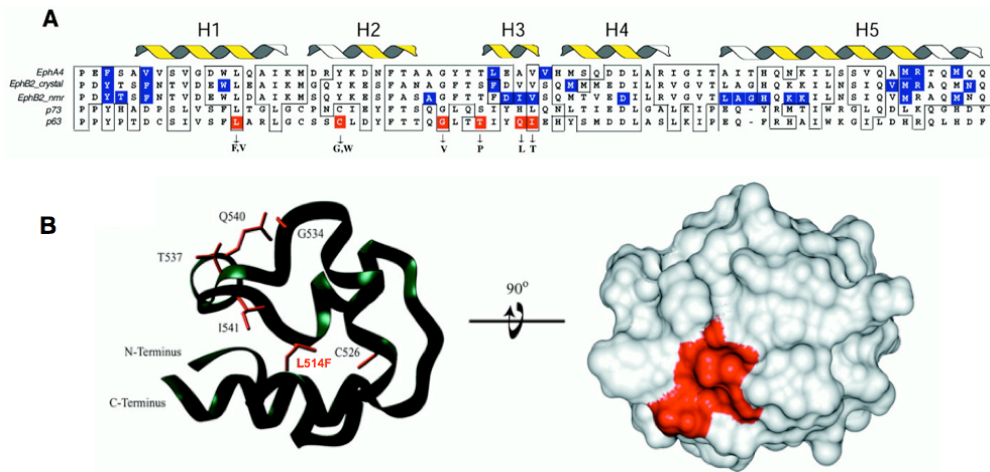


Figure 6. Position of missense mutations in the p63 SAM domain that cause AEC syndrome. (A) Multiple sequence alignment of SAM domains of p63 with SAM domains of other proteins. The five helices are indicated as H1–H5. The white helices are the helices in the Eph receptors and the yellow parts are the helices in p73. Identical and similar amino acids are depicted in white boxes. Residues that are involved in dimerization are highlighted in blue. The mutated amino acids in p63 are indicated with red boxes. (B) Homology model of the p63 SAM domain. A similar five-helical fold is predicted as for p73 and the other SAM domains with known structure. The position of mutated amino acids is indicated in red. On the right is a space-filling representation, showing the clustering of amino acids glycine 534, threonine 537 and glutamine 540 on the surface of the p63 SAM domain. The left panel is a ribbon model turned by 90° that shows the position of all mutated amino acids. Amino acids leucine 514, cysteine 526 and isoleucine 541 are buried inside the SAM domain and are likely to be involved in the proper packing of the helices (Adapted from McGrath et al, *Hay-Wells syndrome is caused by heterozygous missense mutations in the SAM domain of p63*, Hum Mol Genet, 2001).

2. MATERIALS AND METHODS

2.1 Targeting vector

A targeting vector for introducing a T-to-A substitution, which generated a phenylalanine in place of a leucine in 514 position into exon 13 of murine p63 gene locus, was constructed with the bacterial artificial chromosome (BAC) recombineering technique using the recombinogenic bacterial strain EL350 in accordance with procedures described by Liu Pentao (42). The first step consisted in subcloning DNA via gap repair from BAC bMQ-241L2 (Sanger institute, 129S7/AB2.2 BAC clones) into a pBluescript vector. The mouse BAC clone bMQ-241L2 contained an insert of 152,989-bp of genomic DNA from chromosome 16 and included a large part of p63 gene that is about 200,000-bp. Two sets of PCR primers were produced and used to amplify two 500-bp regions of the BAC (*NotI*-p63ex12For: 5'ATAAGCGGCCGC-CAGGATGCTGCTGGTGATAA3' and *HindIII*-p63ex12Rev: 5'GTCAAGCTT-GGAGCCACAATAGCCCTGTA3'; *HindIII*-p63-3'UTRFor 5'GTCAAGCTT-TGCAAAAGCAAATGAGTCCT3' and *SpeI*-p63-3'UTRRev: 5'TCTACTAGT- GGAATCCCATTCTCCACTGA3'). These two regions marked the ends of the fragment to be subcloned via gap repair from the BAC into pBluescript vector. The PCR products were purified using spin columns and digested with either *NotI* and *HindIII* or *HindIII* and *SpeI*. Restriction sites for these enzymes were included in the amplification primers to permit directional cloning of the PCR products into pBluescript cut with *NotI* and *SpeI*. The vector obtained by ligation of miniarms and

pBluescript was subsequently linearized with *HindIII* to create a DNA double-strand break for gap repair. The linearized vector was electroporated into the recombinogenic bacterial strain EL350 in which previously was electroporated the bMQ-241L2 BAC clone. The obtained repaired vector contained exons 12-13-14 and the 3'UTR of p63 gene. In this vector we inserted the L514F point mutation and the positive selection marker PGK-Neo in one recombineering step by electroporating in the EL350 recombinogenic bacterial strain the repaired vector and a linearized DNA fragment containing the PGK-Neo cassette flanked by lox P site and by the regions between which the marker had to be inserted: at 5' by a 250-bp region containing the L514F mutated exon 13 and at 3' by the intron 13. The L514F mutated exon 13 was amplified by PCR from a vector in which previously was cloned and mutagenized, with following primers:

NotI-ex13_for 5'ATAAGCGGCCGC-
CAAATCGCCAGCTGAAAAAT3'

EcoI-ex13_rev 5'GTCGAATTCC-GAGGTTCTGACCTGGAGAG3'

The intron 13 was amplified from the repaired vector with the following primers:

*Bam*HI-intron13 for 5'ATAGGATCCGCAATCAATATGCCTGATCCT3'

*Sal*I-intron13 rev 5'GTCGTCGACTTTCTGCTCTCCTGCCTGAT3'

The PCR amplified regions, after spin columns purification, were digested respectively with *NotI* and *EcoRI* and *Bam*HI and *Sal*I and were ligated in the pL251 vector with the PGK-Neo cassette *EcoRI-Bam*HI cut from this same vector. The resulting minitargeting vector was *NotI-Sal*I digested to obtain the PGK-Neo cassette flanked by the two regions of homology and electroporated in EL350 *E.Coli* bacterial strain together with the repaired

vector containing the p63 sequence. The final vector containing a PGK-neo cassette flanked by lox P sites and the L514F point mutation in the exon 13 was electroporated in mouse E14Tg2A embryonic stem (ES) cells.

2.2 Growing E14Tg2A ES cells

E14Tg2A (BayGenomics) is a feeder independent ES cell line derived from the 129/Ola mice strain. The cells were cultured on 0.1% of gelatin (Sigma) in ES cell medium containing leukocyte inhibitory factor (Chemicon catalog # ESG1107). ES cells were routinely passaged every 2 days and the medium was changed every day.

2.3 Gene Targeting in Embryonic Stem (ES) Cells and Generation of p63^{+L514F} mice

About 3×10^7 ES cells were resuspended in 750 μ l PBS and placed in 0.4 cm cuvettes; 15-25 μ g of targeting vector linearized with *NotI* restriction enzyme, were added to the cells and introduced in ES cells by electroporation (250V 500 μ F) in a Bio-rad gene pulser. After electroporation cells were plated in 6-8 p100 dishes. After 24 hr, the cells were placed under selection with 100 μ g/ml G418 (GIBCO/BRL) for 7 days. Four hundred neomycin-resistant positive ES clones were screened at 3' and 5' of the insertion in the p63 endogenous locus by PCR analysis using an oligo that anneal in the neomycin cassette and an oligo in the

genomic DNA. Screening to 5' of the insertion was performed with the following primers:

EsScreen5'F 5' CAGACTGCAGCATTGTCAGGTGAG 3'

EsScreen5'R 5' GCTAGCTTGGCTGGACGTAAACTC 3'

Screening to 3' of the insertion was performed with the following primers:

EsScreen3'F ATGGCTTCTGAGGCGGAAAGAACCAG

EsScreen3'R AGGCCAGAGGTCAGAAGGATGAACACAC

Only one clone was positive to both 3' and 5' PCR analysis. The homologous recombination event was confirmed by southern blotting.

Genomic DNA, purified from wild-type or putative recombinant ES cells, was digested with *EcoRI* and analyzed with a probe located upstream of the recombinant targeted site. The wild-type allele resulted in a band of 5392-bp. The recombinant ES clone contained the wild-type band as well as a recombinant band of 3216bp, consistently with the homologous recombination event. We also performed southern blotting analysis with a probe that anneal the neomycin coding region, to verify that not more of one copy was inserted in the p63 endogenous locus. The presence of mutation in the endogenous locus was confirmed by the sequencing of genomic DNA. The positive clone was injected into blastocyst embryos that were implanted into pseudopregnant female. We obtained six chimeras in a first injection procedure and ten chimeras in a second injection procedure with different fur coat colours. The chimeras were all tested for germline transmittability by breeding with B6D2F1 mouse strain. To distinguish between wild type and mutant mice, newborn mice were screened for cleft palate (the phenotype is lethal) and by the PCR genotyping.

2.4 Southern blotting analysis

Subconfluent adherent cells were washed 2X with PBS and 2ml/100mm of DNA lysis buffer were added (100mM NaCl, 50mM Tris-HCl, pH8, 100mM EDTA, pH8, 1%SDS, 1mg/ml Proteinase K). Cells were incubate 2-3 hours in culture dish at 55°C.

Genomic DNA was extracted with phenol (pH 8.0) 2X. DNA samples were shaken for some minutes in order to avoid a long contact of DNA with phenol and spinned in Sorvall 10' at 10000 rpm; after chloroform extraction 2X (same procedure as for phenol), DNA was washed in 70% ethanol, dried and resuspended in 1ml TE by rotating sample few hours at r.t. About 14 µg of DNA were digested in a total volume of 150µl with $\geq 5U/\mu g$ of *EcoRI* (or *BglII*, *HindIII*, *EcoRV* in the case of southern blotting with the probe that anneal on neomycin cassette) enzyme o/n. Following a first Phenol/ Chloroform extraction, purified DNA was digested again in a total volume of 100µl with $\geq 5U/\mu g$ of appropriate enzyme for ~4-5 hours. After a second Phenol/ Chloroform extraction, DNA samples were washed, dried for max. 10 minutes; 15µl of H₂O were added and DNA was resuspended at 65°C for 10-15 minutes. Samples were loaded on 0.7% agarose gel and run at ~35mA o/n. The day after the agarose gel was placed in a tray with 250-500ml of HCl solution (21.6ml HCl/1 liter ddH₂O) and incubated 2 X 15' at r.t. to nick DNA and facilitate the transfer of DNA bands on nylon membrane. Then the gel was rinsed 2X with ddH₂O and soaked 20-30' 2X in a fresh denaturing solution (1.5M NaCl, 0.5M NaOH). Finally agarose gel was soaked 20-30' 2X in neutralization solution (1M Tris pH7.2, 3M NaCl).

DNA bands were transferred from the agarose gel to a nylon membrane by placing the membrane on top of gel and filling the blotting tray with 20X SSC. After 24 hours the blotting pads were stacked and the nylon membrane was UV crosslinked in Stratalinker (stratagene). The membrane was prehybridized with 43% Formamide 5X, SSC 0,2%, SDS 50 mM, Phosphate buffer pH 7.0, 5X Denhardt solution, 400 µg/ml yeast tRNA, 50 µg/ml Salmon sperm o/n. Then the membrane was incubated o/n with the radiolabeled probe prepared using Amersham rediprime kit for random prime labeling. The day after the membrane was washed twice, 10 minutes each, with a low stringency wash (2x SSC, 0.1% (w/v) SDS), then with a medium stringency wash (1x SSC, 0.1% (w/v) SDS) for 15 minutes and finally twice, 10 minutes each, with a high stringency wash (0.1x SSC, 0.1% (w/v) SDS). The membrane was exposed to X-ray film for 24-48 hours.

2.5 Mouse genotyping

p63^{+L514F} mutant mice are genotyped by PCR using genomic DNA isolated from mouse tails. Primers used for amplification of wild-type allele were:

Screen-ex13L514F-For 5'-GTCTGACCTCCCGACCCACCTCCT-3'

Screen-ex13L514-wild-type-Rev 5'-

GCATGATGAGCAGCCCAACCTTGCT-3'

Primers used for amplification of mutant allele were:

Screen-ex13L514F-For 5'-GTCTGACCTCCCGACCCACCTCCT-3'

Screen-ex13L514F-Mut-Rev 5'-

GCATGATGAGCAGCCCAACCTTGCA-3'

Forward primer was in common while the reverse primer differed only at 3' for the presence of the point mutation. Genomic DNA from p63^{+L514F} was amplified by both couples of primers, whereas genomic DNA from wild-type littermates was amplified only by the oligo reverse with the correct base in 3' first position.

2.6 Histopathology and Immunostaining

Dorsal skin were dissected, fixed in 4% paraformaldehyde (PFA) and embedded in paraffin or in OCT, from which 7 µm sections were cut and stained with Haematoxylin and Eosin (H&E) or by immunohistochemistry according to standard methods. For paraffin sections, permeabilization for antigen retrieval was performed by microwaving samples in 0.01 M citrate buffer at pH 6.0. The following antibodies were used: rabbit antibodies to keratin 6, keratin 14, keratin 1, involucrin, loricrin (all Convance), Caspase 3 active (R&D system), mouse antibodies to BrdU G3G4 (originally provided by Dr. Steve J. Kaufman, Illinois and maintained by the Developmental Studies Hybridoma Library, University of Iowa), p63 (4A4, Santa Cruz Biotechnology), alpha tubulin (Sigma), rat antibody to E-cadherin (Zymed laboratories-Invitrogen), goat antibody to IGF2 (R&D system), guinea pig antibody to keratin 15 (a gift from Langbein). The following secondary antibodies were used for immunofluorescence staining: Alexa Fluor ® 488 goat anti-mouse (Invitrogen), Alexa Fluor ® 594 goat anti-rabbit (Invitrogen), Alexa Fluor ® 594 goat anti-rat (Invitrogen). Fluorescent signals were monitored under a Zeiss Axioskop2 plus image

microscope or under a Zeiss confocal microscope LSM510meta.

2.7 Western Blot

For immunoblotting cells were lysed in sample buffer (10% glycerol, 0.01 % Bromophenol Blue, 0.0625 M Tris-HCl pH 6.8, 3 % SDS, 5 % β -mercaptoethanol) supplemented with protease inhibitors. For immunoblotting of epidermal extracts, epidermis was isolated from dermis by producing a termic shock at 55°C or by floating skin biopsies, epidermis side up, in a 0.5 M ammonium thiocyanate (NH_4SCN) in phosphate buffer, pH 6.8 (0.1 M Na_2HPO_4 , 0.1 M KH_2PO_4) for 20 min on ice. After isolation from dermis, epidermis was snap frozen in liquid nitrogen and then homogenized with a polytron in lysis buffer supplemented with phosphatase and protease inhibitors. Twenty-five micrograms of protein per lane were run on a denaturing SDS-PAGE gel and subsequently transferred to Immobilon-P transfer membranes (Millipore) probed with primary antibodies and detected by chemiluminescence (ECL, GE Healthcare Life Sciences). Antibodies used for immunoblotting were rabbit anti-total-AKT, rabbit-phospho-AKT^{Ser}, rabbit anti-phospho-p44/42 MAPK and rabbit anti-total-p44/42 MAPK (1:1,000; Cell Signaling Technologies) and those listed above. Secondary antibodies included donkey anti-rabbit IgG and sheep anti-mouse IgG conjugated to horseradish peroxidase (HRP) (1:2000; Amersham Biosciences), as well as donkey anti-goat HRP and goat anti-rat HRP (1:1000; Santa Cruz Biotechnology). To detect multiple proteins, membranes were treated in stripping buffer (100 mM β -mercaptoethanol,

2% SDS, and 62.5 mM Tris [pH 6.8]) and then reprobed.

2.8 BrdU incorporation assay

Cells were labeled with 5-bromo-2-deoxyuridine (BrdU, Zymed, 1:100) for 3 hrs, and then fixed in 4% PFA, washed in phosphate-buffered saline (PBS), treated with 50mM NaOH, and permeabilized in 0.1% NP-40. Cells were subsequently incubated with anti-BrdU antibody listed above (1:500) in the presence of DNase (0.2 mg/ml, Sigma) and detected by immunofluorescence using Alexa Fluor® 488 goat anti-mouse (Invitrogen). For *in vivo* analysis, BrdU was injected (1ml/100g body weight) intraperitoneally in pregnant mouse females and incubated for 3hrs. Embryos were taken at E13.5, E16.5 and P0 stages, fixed in 4% PFA, and embedded in paraffin. 7µm sections were permeabilized in 0.2% Triton X-100, and processed for immunofluorescence as described above.

2.9 Skin Barrier Assays

To perform X-gal staining, unfixed, untreated newborn mice or embryos were washed in PBS and then incubated overnight at 37°C in 5-bromo-4-chloro-3-indlyl-b-D-galactopyranoside (X-gal) reaction mix (100 mM NaPO₄, 1.3 mM MgCl₂, 3 mM K₃Fe[CN]₆, 3 mM K₄Fe[CN]₆, and 1 mg/ml X-gal [pH 4.5]). At pH 4.5, the skin exhibits endogenous b-galactosidase activity, so increased X-gal staining indicates epidermal permeability to X-gal, a sign of compromised barrier function (43).

2.10 Primary keratinocytes

Newborn mice were placed in petri dishes with ice and inserted in an ice bucket. After 30-45' newborn mice were washed twice with 70% ethanol and twice with water to remove ethanol completely. Using sterile techniques, mice tails and limbs were amputated with sterile surgical scissors. The skin was carefully separated from the rest of the viscera and flattened in a empty 150mm petri dish with the dermis facing down; 20 ml of Dispase solution (Roche) were added to each petri dish and incubated o/n at 4 °C. Next day epidermis was separated from the dermis and placed in a 100mm Petri dish in 2,5ml (for each epidermis) of 0.125% trypsin-2.5mM EDTA. Epidermis was minced with tweezers and scissors until is reduced in very small fragments and placed at 37°C for 5-8 minutes. Then trypsin is inactivated with DMEM+10% FBS and filtered by applying it to a gauze in order to remove the floating particles. Cells were placed into the centrifuge for 5 minutes at 1000 rpm; then were plated on collagen coated plates (2×10^6 cells/ml) and incubated at 34°C, 8% CO₂.

2.11 Colony-forming assays

About 10^3 cells/cm² were plated on 35mm dishes coated with 2mg/35mm dish of Matrigel (BD Bioscience) in Defined PCT-Epidermal keratinocytes medium (CellnTec advanced cell system); keratinocytes were cultured for three weeks. Then cells were washed in PBS and stained with Crystal violet for 10 minutes.

2.12 Real-time RT-PCR

Total RNA was extracted from primary keratinocytes or epidermis (isolated from the dermis with the method described above) using TRIzol reagent (Invitrogen). RNA samples were treated with RNase-free DNase I (Promega), and cDNA was synthesized using SuperScript Vilo (Invitrogen). Two-step real-time reverse transcription RT-PCR was performed using the SYBR Green PCR master mix in an ABI PRISM 7500 (Applied Biosystems). Levels of the target genes were quantified using specific oligonucleotide primers and normalized for Actb (β -actin) expression.

2.13 Fluorescent activated cell sorting (FACS) analysis

Keratinocytes were isolated from newborn mice with the procedures described (see paragraph “*Primary keratinocytes*”) and stained for one hour with both CD49f and CD71 primary antibodies (BD Bioscience). For each sample at least 10000 events were acquired with FACSCanto II Flow Cytometry System (BD Biosciences), and analyzed with the ModFit LT 3.0 software (Verity Software House).

2.14 Gene expression microarrays

We measured the differential expression of 22000 RNA on freshly isolated epidermis from three mutant versus three wild-type newborn mice. We hybridized the RNA samples to the Affymetrix Mouse Genome 430A 2.0 chips. We processed the microarrays using the RMA algorithm. False

Materials and Methods

Discovery Rate (FDR) correction was performed on the estimated p-value to correct for multiple hypothesis test.

3. RESULTS

3.1 Generation of a mouse model carrying the L514F AEC human mutation

We generated a knock-in mouse model for AEC syndrome by inserting the L514F point mutation, that has been found in a number of AEC patients (28), in an otherwise wild-type p63 gene. The targeting vector was created through BAC recombineering using the recombinogenic bacterial strain EL350 (42).

This vector contains the L514F point mutation in the exon 13 that encodes for the SAM domain (see Introduction) and the positive selection marker PGK-Neo flanked by lox-P sites for Cre-recombinase mediated removal. The mutation was introduced by homologous recombination (knock-in strategy) in the *p63* gene locus of mouse embryonic stem (ES) cells E14Tg2A (BayGenomics), a feeder independent ES cell line derived from the 129/Ola mice strain (Fig. 7A).

We extensively validated the homologous recombination event by PCR and Southern blotting. The genome of the ES positive clone was sequenced to confirm the presence of mutation (Fig. 7B). Then, blastocysts injected with mutant ES cells, were transferred into pseudopregnant C57BL/6 female. We obtained six chimeras in a first injection procedure and ten chimeras in a second injection procedure. After we have tested their transmittability, chimeric mice carrying the L514F AEC mutation were mated with wild-type B6D2F1 mice to obtain $p63^{+/L514F}$ heterozygous mice.

Results

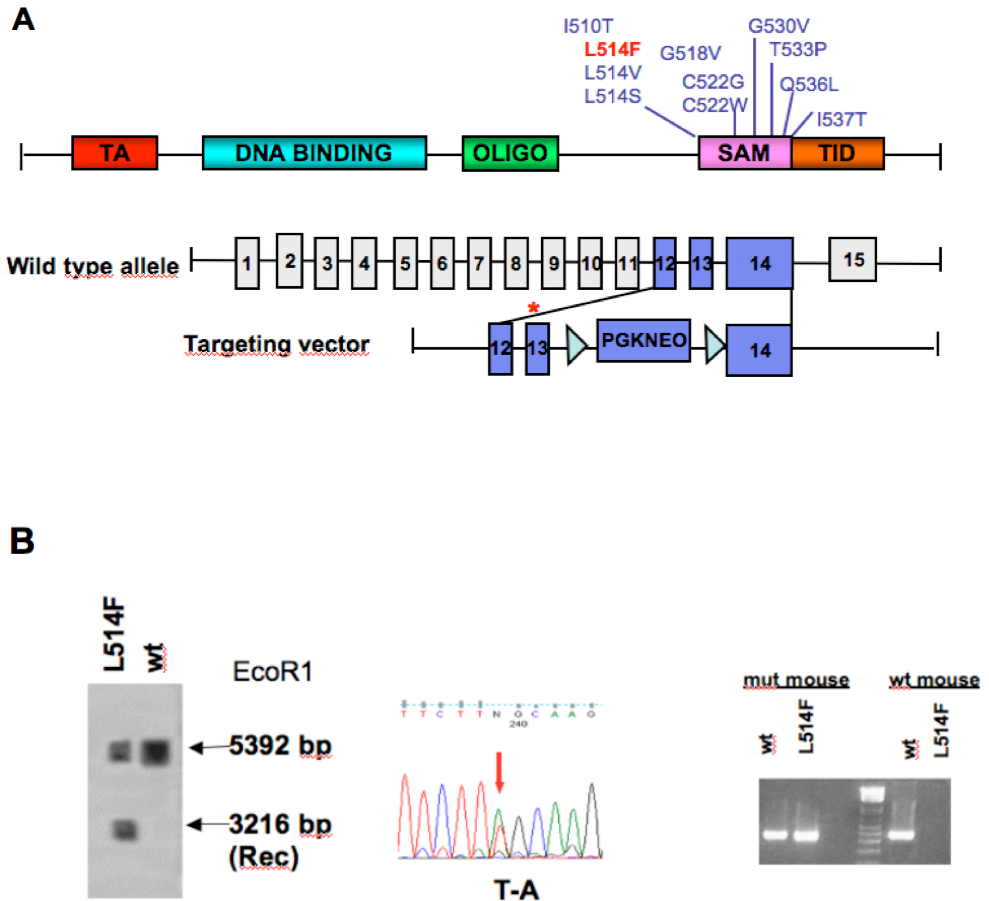


Figure 7. Generation of the $p63^{+/L514F}$ knock-in mouse model. **A.** The L514F human mutation (*) was inserted in exon 13 of the p63 gene, that encodes the SAM domain. A PGK-neo positive selection cassette, flanked by loxP site, was placed downstream of exon 13. **B.** Left panel: Genomic DNA, purified from wild-type (wild-type) or L514F ES cells were digested with *EcoRI* and analyzed with a probe located upstream of the recombinant targeted site. The wild-type allele results in a band of 5392bp. The L514F ES clone contained the wild-type band as well as a recombinant band (Rec) of 3216bp, consistently with the homologous recombination event. The mutation was confirmed by sequencing genomic DNA. Right panel: The L514F mutation in the $p63^{+/L514F}$ mouse DNA was detected by PCR analysis using primers for either the mutated or the wild-type sequence.

3.2 $p63^{+/L514F}$ mice recapitulate the phenotype of AEC patients

$p63^{+/L514F}$ mice died within 12 hours after birth; the cause of death is the severe cleft of the secondary palate that results in stomach and intestine filled with swallowed air and complete absence of milk in the stomach (Fig. 8A-B). Facial processing fused properly at early stages of development so that mice were not affected by cleft lip (Fig. 8A).

During development in $p63^{+/L514F}$ mice the palate shelves elevated, but do not come in close proximity to fuse and form the secondary palate. In humans this defect is compatible with life and can be treated surgically.

$p63^{+/L514F}$ mice showed skin defects, ectodermal dysplasia, including defects in tooth and hair development, epidermal and hair follicle hypoplasia and no limb abnormalities, thus faithfully recapitulating the defects observed in AEC patients.

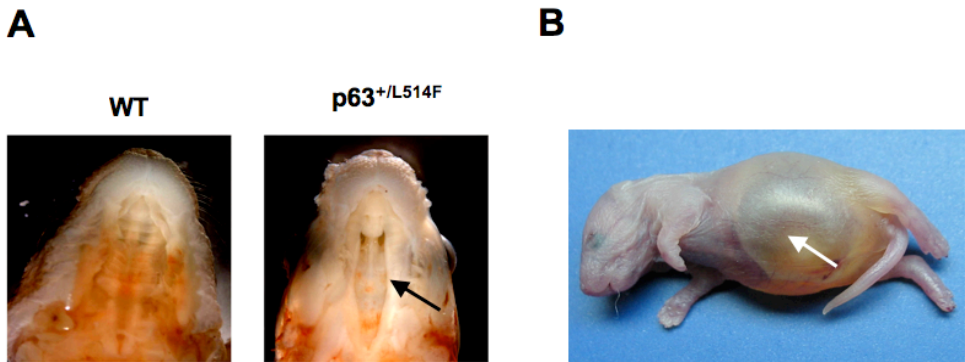
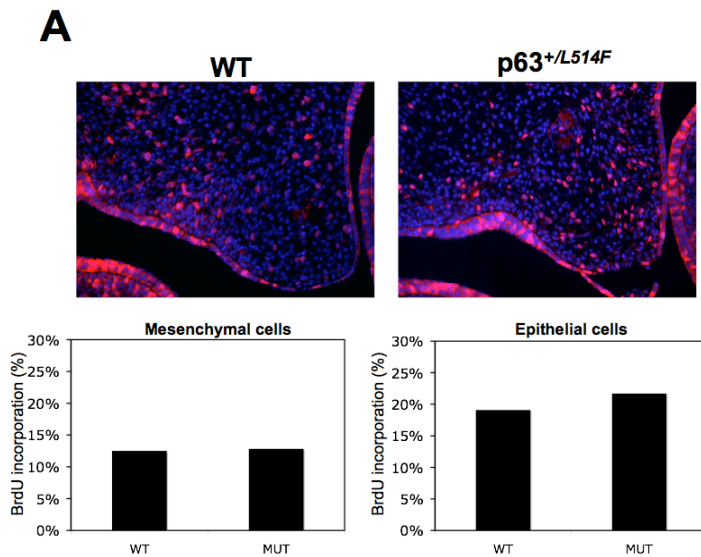


Figure 8. Cleft palate of $p63^{+/L514F}$ mice. **A.** Cleaving affected the hard palate (secondary palate) as indicated by the black arrow. **B** cleft palate was responsible for dehydration since mice were unable to take milk and for bubble in the stomach (white arrow) due to inability to breathe.

Results

We performed a BrdU incorporation analysis on two $p63^{+/L514F}$ versus two wild-type mice at E13.5 and we found that proliferation of mesenchymal and epithelial cells was not affected by the mutation (Fig.9A). Thus, our preliminary result indicated that elevation and reorientation of palatal shelves at E13.5 occurred properly. A larger number of mutant and wt mice will be necessary to analyze in order to confirm this result.

Haematoxylin and Eosin (H&E) staining on palatal section of $p63^{+/L514F}$ and wild-type mice at E14.5 and E15.5 showed that the defect is detectable at E14.5 because the opposing palatal shelves fail to meet in the horizontal plane; it persists at E15.5, when the palatogenesis was complete in wild-type mice, and after birth (Fig. 9B



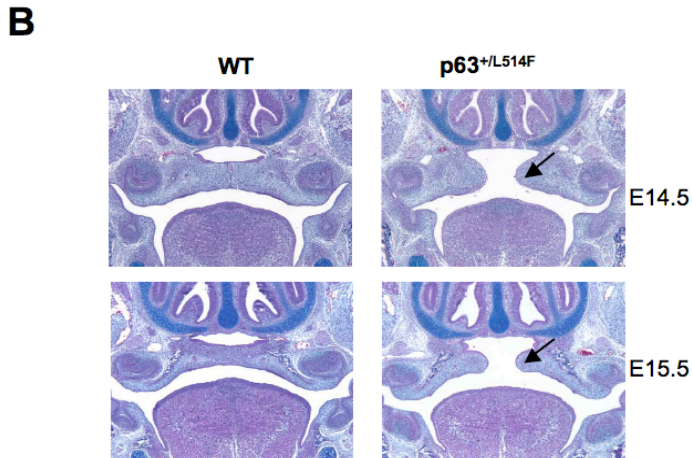


Figure 9. Mutant palatal shelves do not come in contact. **A.** BrdU incorporation analysis on E13.5 $p63^{+/L514F}$ versus wild-type embryos showed correct proliferation of mesenchymal and epithelial cells of palatal shelves. Charts below: quantification of the percentage of BrdU positive mesenchymal and epithelial cells **B.** H&E staining showed that palatal shelves fail to meet in the horizontal plane at E14.5; the defect persists at E15.5 (black arrow) and until the birth.

We mainly focused our attention on skin phenotype. We performed H&E staining on several skin sections isolated from the of $p63^{+/L514F}$ and wild-type mice and we found an overall reduction in skin thickness, accompanied by a significant epidermal and hair follicle hypoplasia with a penetrance of 100% (Figure 10A).

The vast majority of $p63^{+/L514F}$ mice did not display skin erosions at birth, but their epidermis was fragile and easily broke above the basal layer during histological processing (Figure 10B).

We measured the epidermal thickness from the basal lamina to the granular layer. Measurement was performed on six $p63^{+/L514F}$ versus *wild-type* skin

Results

sections of newborn mice stained with H&E. We found a highly significant reduction in epidermal thickness of about 50% (Fig. 10C).

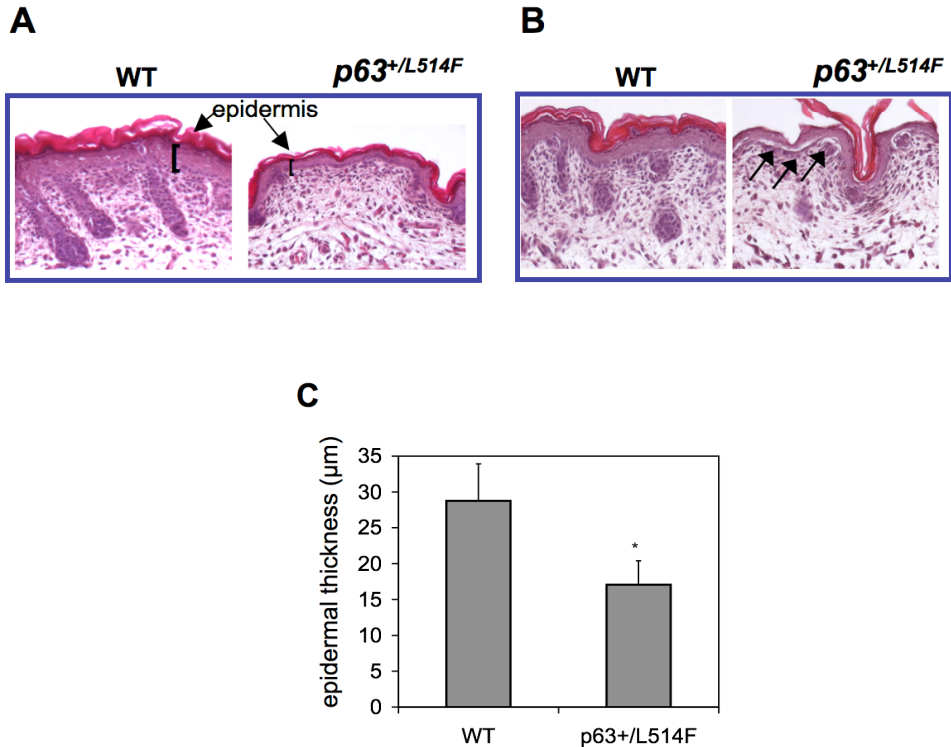
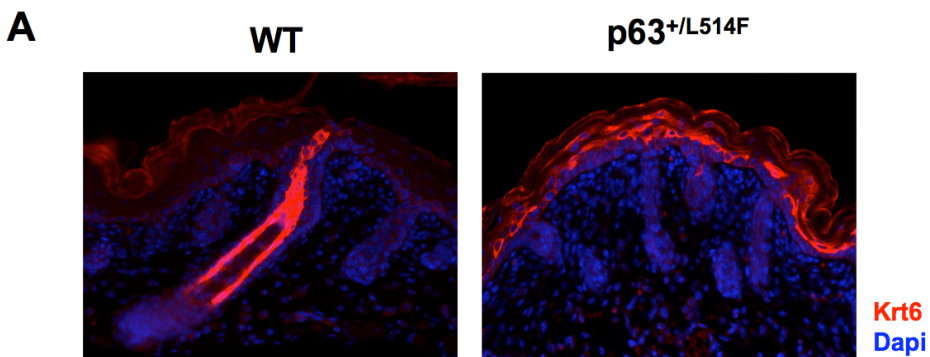


Figure 10. Skin hypoplasia and fragility in $p63^{+/L514F}$ mice. **A.** H&E staining of skin sections at birth; Black arrows indicate the epidermal thickness of mutant versus wild-type skin. **B.** Focal epidermal gaps between the basal and the spinous layers of the epidermis (black arrow). **C.** Measurements of epidermal thickness in wild-type and $p63^{+/L514F}$ skin at birth. * indicates a statistically significant difference (p -value=0.0009 ($n=6$)).

Results

Epidermal alteration in our mouse model was confirmed by the ectopic expression of Keratin 6 (Krt6). We found a variable increase in protein production by immunoblotting analysis performed on epidermal extract of *wild-type* and $p63^{+/L514F}$ newborn mice skin (Fig.11A) and an induction of Krt6 in the differentiating layers of $p63^{+/L514F}$ mice by immunofluorescence staining (Fig. 11B). Under physiological condition Krt6 is expressed in the companion layer, matrix, and medulla of anagen-stage hair follicles, but not in epidermis (44, 45). Injury to stratified epithelia causes a strong induction of Krt6 in post-mitotic keratinocytes located at the wound edge. The induction occurs within 6 h after injury to human epidermis. Its subsequent accumulation in keratinocytes correlates with the profound reorganization of keratin filaments in suprabasal keratinocytes, followed by alteration in their shape and cell-cell adhesion. These changes coincide with the onset of re-epithelization (46). Although $p63^{+/L514F}$ mice did not display detectable lesions we found an increase in Krt6, consistent with the possibility that $p63^{+/L514F}$ mice die before the skin fragility phenotype evolves in detectable lesions.



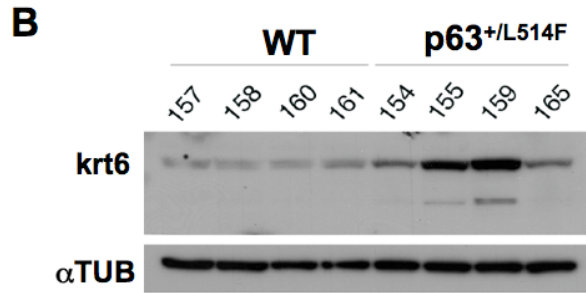


Figure 11. Expression of Krt6 on epidermis of wild-type and p63^{+L514F} newborn mice. **A.** Immunofluorescence staining with an antibody against Krt6 showed an aberrant expression in the differentiating layers of mutant epidermis. **B.** Immunoblotting of epidermal extracts with Krt6 showed an increased production of this protein in mutant mice; α -TUBULIN (α TUB) was used to normalize samples.

3.3 Global gene expression profile of $p63^{+/L514F}$

To obtain a global view of changes in gene expression of $p63^{+/L514F}$ mice, we performed a comparison of gene expression profiling of mutant versus wild-type epidermis at birth using Affymetrix gene chip. We found 63 downregulated and 23 upregulated transcripts in AEC mutant epidermis versus wild-type (FDR<0.2, 2 fold induction). Six genes are putative direct targets of p63 as suggested by previous ChiP-chip experiment (47, 48). Interestingly, a number of bona-fide direct p63 target genes, including Perp (49), Keratin14 (Krt14) (50), and Redd1 (51), were unaffected in mutant epidermis, and only a limited number of genes were differentially expressed in $p63^{+/L514F}$ versus wild-type epidermis, the vast majority of which were also affected by p63 knockdown in keratinocytes. These data indicated that defects in $p63^{+/L514F}$ mice involve likely as-yet poorly explored cellular mechanisms downstream of a specific subset of p63 target genes. The basal layer keratins Krt14 and Keratin 5 (Krt5), and the main suprabasal keratins Krt1 and Krt10 whose expression was lost in $p63^{-/-}$ mice, were essentially unaffected in $p63^{+/L514F}$ mice at least at birth. In contrast, mRNA expression of a number of other keratins typical of the epidermis was inhibited at birth, including Keratin 15 (Krt15), Keratin2 (Krt2) and the poorly characterized Keratin 79 (Krt79). Interestingly Krt79 in humans is highly expressed in the scalp (52), the main site of skin erosions in AEC patients. In parallel with reduced expression of some epidermal keratins, $p63^{+/L514F}$ epidermis displayed increased focal expression of other keratins, including Krt6 (Fig.11) and Keratin 16 (Krt16) that are essential to maintain keratinocyte integrity in wounded epidermis (45), and Keratin 8 (Krt8) and Keratin 18 (Krt18), simple epithelial keratins, that for their nature can participate to

Results

intermediate filaments but do not confer strong mechanical resistance to the epithelium (data not shown). Interestingly, Krt15 was strongly reduced at the protein level both in the epidermis and in the bulge of hair follicle at birth (Fig.18B), whereas Krt6 was aberrantly expressed in $p63^{+/L514F}$ epidermis (Fig.11A-B).

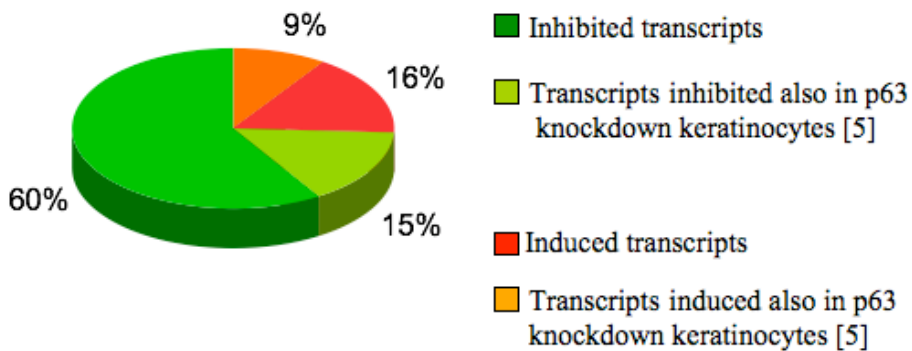


Figure 12. Global gene expression profile of $p63^{+/L514F}$. Comparison of gene expression profiling of newborn $p63^{+/L514F}$ versus *wild-type* epidermis using Affymetrix gene chips. 85 transcripts (2-fold; FDR<0.2) are significantly altered in mutant epidermis. Most bona-fide direct p63 target genes are unaffected in mutant epidermis.

3.4 Epidermal proliferation and differentiation are not affected in $p63^{+/L514F}$ mice

During embryonic development several alterations can be responsible for skin fragility in $p63^{+/L514F}$ mice since p63 has been involved in different biological processes including maintenance of cell proliferation (53, 54), induction of stratification and inhibition of terminal differentiation (55, 56). We tested whether these functions were affected in $p63^{+/L514F}$ mutant skin. We measured epidermal cell proliferation by performing a quantitative BrdU incorporation assay on $p63^{+/L514F}$ versus wt mice at birth and during skin maturation (E13.5, E16.5, and P0) (Fig.13A). Quantification of BrdU positive epidermal cells showed that the proliferation rate of mutant epidermal cells was comparable to that of wild-type. We obtained the same results by performing BrdU incorporation assay on cultured primary keratinocytes isolated from either $p63^{+/L514F}$ or wild-type epidermis (Fig. 13B).

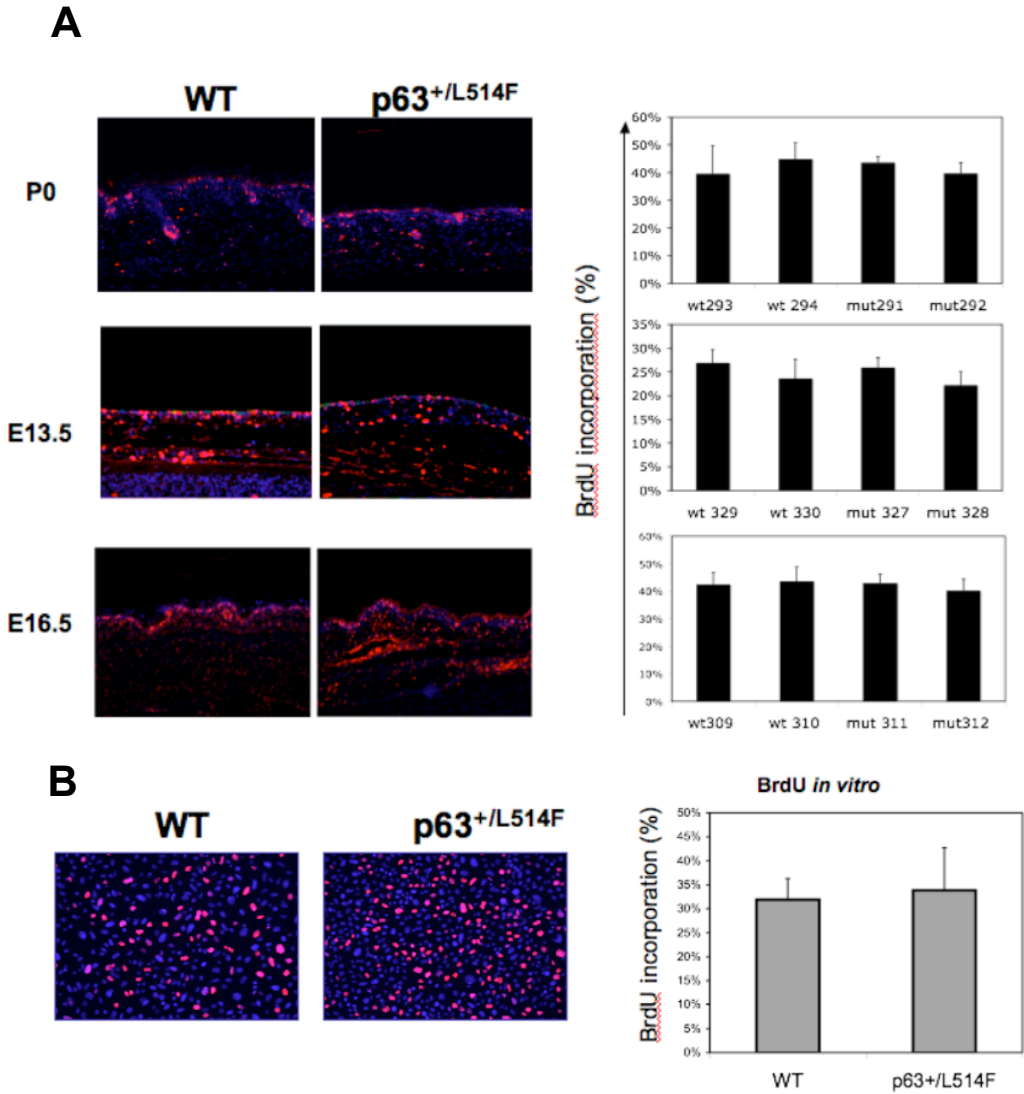
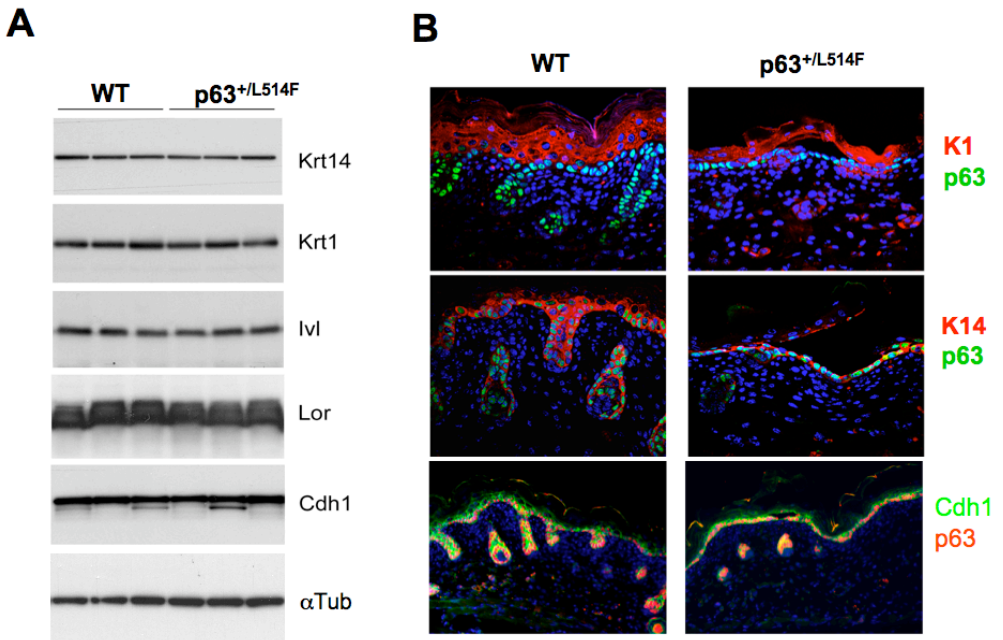


Figure 13. Cell proliferation is unaffected in p63^{+/L514F} skin. **A.** Left: immunofluorescence staining of skin in newborn mice (P0), at E13.5 and E16.5 with BrdU (in red) specific antibody. Left: Quantification of BrdU positive epidermal cells **B.** Right: BrdU staining on keratinocytes isolated from wild-type and p63^{+/L514F} epidermis. Left: Quantification of BrdU positive keratinocytes.

Results

To determine if epidermal differentiation was affected by L514F AEC mutation, we performed immunoblotting analysis on epidermal extracts from either wild-type or $p63^{+/L514F}$ mice with E-cadherin (Cdh1), a component of the adherent junction; Keratin 14 (Krt14), a marker of the basal layer; Keratin 1 (Krt1), a marker of the spynous layer and Involucrin (Ivl) and Loricrin (Lor), markers of terminal differentiation and we did not find any obvious differences between wild-type and $p63^{+/L514F}$ protein levels (Fig.14A). Immunofluorescence analysis on either wild-type or $p63^{+/L514F}$ epidermis showed that all markers localize properly (Fig.14B). Accordingly, the epidermal barrier was not significantly altered at E17.5 as indicated by permeability assay performed on wild-type and mutant embryos (Fig. 14C).



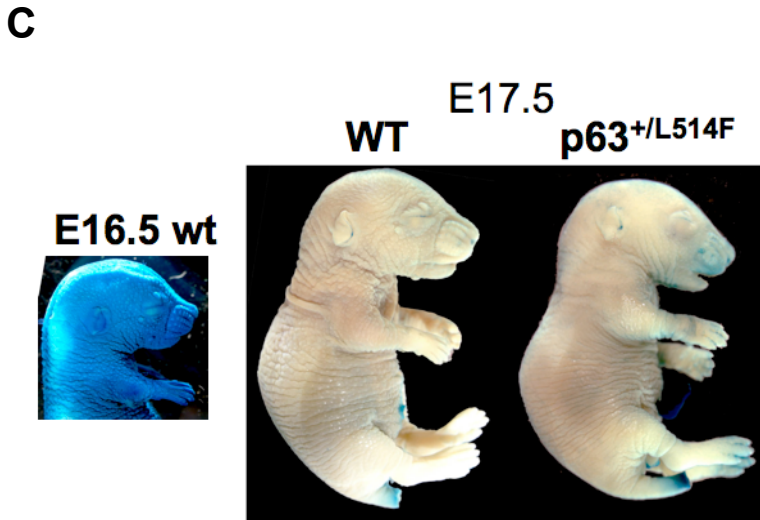


Figure 14. Epidermal differentiation of p63^{+/L514F} mice. **A.** Immunoblotting analysis of several differentiation markers on epidermal extracts collected at birth from three wild-type and three p63^{+/L514F} mutant mice. Krt14: Keratin 14. Krt1: Keratin 1. Iv1: involucrin. Lor: Loricrin. Cdh1: E-cadherin; α TUB is used to normalize samples. **B.** Immunofluorescence staining on skin section of newborn mice with Krt14, Krt1, Cdh1, shows a correct localization of these markers in epidermis. **C.** Permeability assay using X-gal substrate on wild-type and p63^{+/L514F} mice at E17.5 shows a complete skin barrier formation. Wild-type control embryos have an incomplete barrier at E16.5.

We also evaluated differentiation at E16.5 since a delay during development could be responsible for incomplete stratification at birth. H&E staining on skin section from E16.5 p63^{+/L514F} and wild-type mice showed skin hypoplasia (Fig.15A). Immunofluorescence staining showed the proper expression and localization of Cdh1, a component of the adherent junction

Results

and Krt10, a marker of the spinous layer. Thus, epidermal differentiation of $p63^{+/L514F}$ mice was unaffected.

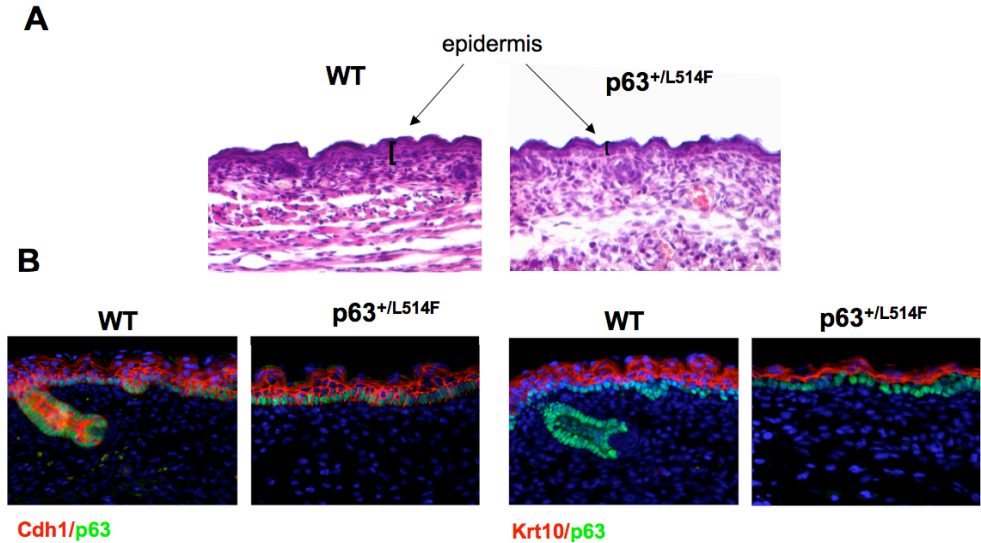


Figure 15: Phenotype of $p63^{+/L514F}$ at E16.5. **A.** H&E staining of skin sections at E16.5. Note the reduction of skin and epidermal thickness in $p63^{+/L514F}$. In spite of this reduction, immunofluorescence analysis displayed a correct expression and localization of epidermal markers. **B.** Immunofluorescence staining of $p63^{+/L514F}$ mice skin sections at E16.5 with Krt10, a marker of the spinous layer, indicates that differentiation occurred correctly.

3.5 Defective proliferative potential of epidermal stem cells in AEC syndrome

Epidermal stem cells are not localized in a specific niche but are interspersed with transit amplifying cells in the basal layer (see Introduction). Wild-type epidermal stem cells are thought to give rise to both transit-amplifying (TA) cells and stem cells at each cell division, which contributes to the logarithmic expansion of epithelial tissues. In contrast, the absence of p63 leads to a decrease of proliferative potential of epithelial stem cells (57). To investigate the effect of L514F on this p63 function we performed colony forming assay, FACS analysis and immunodetection of a putative skin stem cell marker.

3.5.1 Colony-forming assay

To analyze self-renewal ability of $p63^{+/L514F}$ epidermal stem cells, we cultured for three weeks mutant versus wild-type keratinocytes in a medium that favors the growth of epidermal stem cells and subsequently we stained colonies with crystal violet (Fig.16A). Clones were divided in three populations on the basis of their size. We found that clones larger than two millimeters were only the five percent of mutant versus about the thirty-five percent of wild-type clones (Fig.16B). We repeated this assay three times and the result was consistent with a decrease in number and size of $p63^{+/L514F}$ versus wild-type epidermal clones. One week after the beginning of the experiment, $p63^{+/L514F}$ clones showed a different morphology compared to wild-type as indicated by microscopic images (Fig.16C). We

Results

are investigating if this morphology is attributable to a premature apoptosis or senescence of keratinocytes or to an accelerated terminal differentiation.

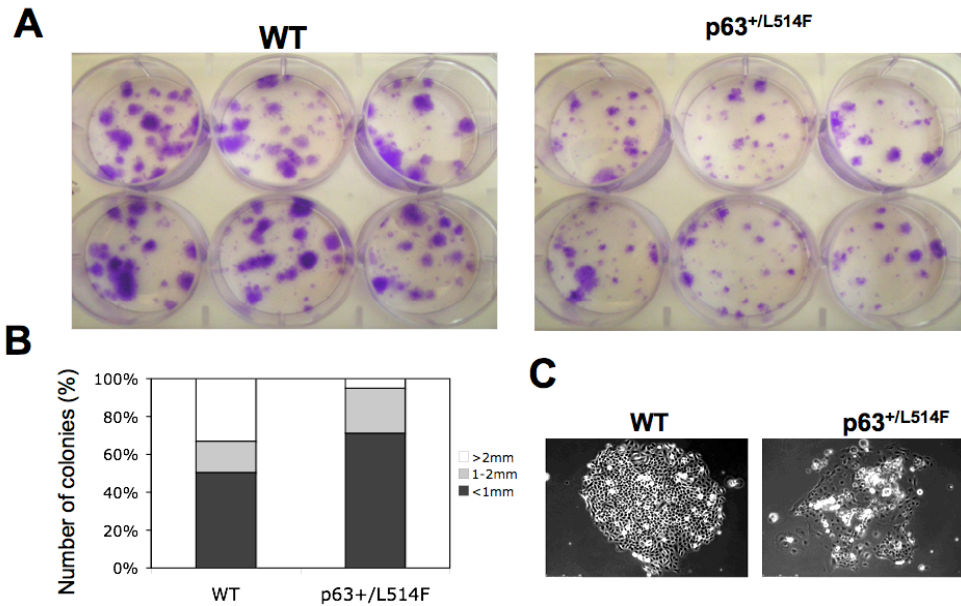


Figure 16. Colony-forming assay. **A.** Colony-forming assay on primary keratinocytes isolated from wild-type and p63^{+/L514F} mutant newborn mice and plated at clonal density for three weeks in a medium that favours growth of epidermal stem cells. **B.** Quantification of the colony-forming assays shown in (A). **C.** Microscope images of wild-type and p63^{+/L514F} keratinocytes at 7 days after plating.

3.5.2 FACS analysis to define epidermal stem cell population

To test whether epidermal progenitor cells derived from $p63^{+/L514F}$ mice have a reduced proliferative potential, we determined the properties of freshly dissociated basal keratinocytes of mutant versus wild-type epidermis by FACS analysis, which allowed us to distinguish putative stem cells and measure their physical characteristics and their cell cycle status. As mentioned in the introduction, epidermal stem cells have not been clearly identified; however, integrin α_6 (CD49f) and transferring receptor (CD71) are used as epidermal stem cell markers (7). A number of reports suggest that the cell fraction characterized by high level of CD49f and low level of transferring receptor CD71 is enriched for cells with characteristics of progenitors (58, 59).

Freshly isolated epidermal cells derived from newborn $p63^{+/L514F}$ mice and their wild-type counterparts were used in this assay. We determined the number of putative stem cells, their physical properties including size and nuclear-to-cytoplasmic ratio, and their cell cycle status, as compared to the total population of basal cells (CD49f^{medium/high} cells). Keratinocytes gated as CD49f^{bri}/CD71^{dim} correspond to a cell population with the smallest cell and nuclear size and exhibited a high nuclear-to-cytoplasmic ratio consistent with the characteristics of a primitive cell type. We found that keratinocytes isolated from $p63^{+/L514F}$ mice were strongly defective in this cell population without any changes of cell cycle parameters (Fig. 17A-B).

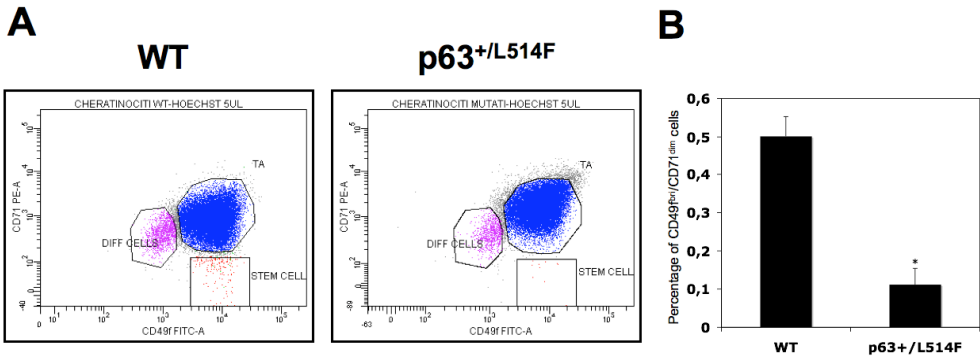


Figure 17. Epidermal stem cells from epidermis of newborn mice. A. Cells freshly harvested from epidermis of wild-type and p63^{+/L514F} mice were subsetted on the basis of CD49f (c, x axis) and CD71 (c, y axis) surface phenotype into fractions enriched for Stem cells (orange) and TA cells (blue). In the panel differentiated cells (pink) are also displayed. **B.** Percentage of stem cells in the epidermis of five different p63^{+/L514F} and wild-type mice. * indicates a statistically significant difference (p-value=0.001 (n=5)).

3.5.3 Expression of the skin stem cell marker *Krt15*

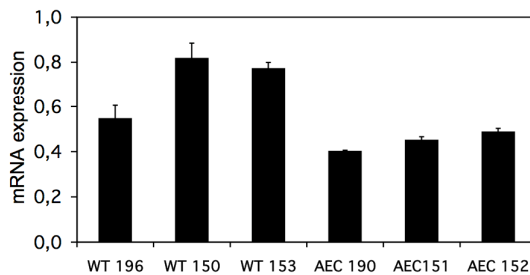
Krt15 is a protein with a poorly understood role in epidermis. It is a marker of the proliferative compartment of epidermis (60, 61). Flow cytometric analysis revealed preferential expression of this keratin in CD49f^{bri} cells (60). In addition, patterns of *Krt15* expression and promoter activity change with age and correlate with levels of differentiation within the cutaneous epithelium. In newborn mice *Krt15* is expressed in the basal compartment of epidermis, whereas its expression becomes restricted to the bulge area in the adult mice (62).

Results

Real time PCR analysis performed on RNA extracted from epidermis of $p63^{+/L514F}$ newborn mice and in their *wild-type* counterpart showed a decrease in Krt15 expression (Fig.18A). This decrease was confirmed also at protein level as showed by immunoblotting and immunofluorescence analysis (Fig.18B).

Real time PCR analysis performed on RNA extracted from several AEC patients with different mutations showed a strong decrease of Krt15 mRNA expression (Fig.19A). Immunofluorescence analysis for Krt15, performed on other AEC patients, confirmed the reduction at protein level (Fig.19B).

A



B

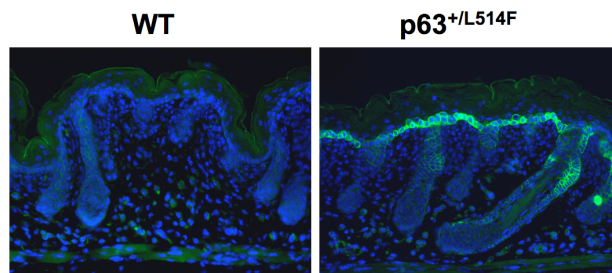


Figure 18. Krt15 is reduced in $p63^{+/L514F}$ newborn skin at both mRNA and protein levels. A. Real time PCR analysis on mRNA from different wild type (WT) and $p63^{+/L514F}$ mice (AEC). **B.** Immunofluorescence staining for Krt15 on backskin section of wt and $p63^{+/L514F}$ mice.

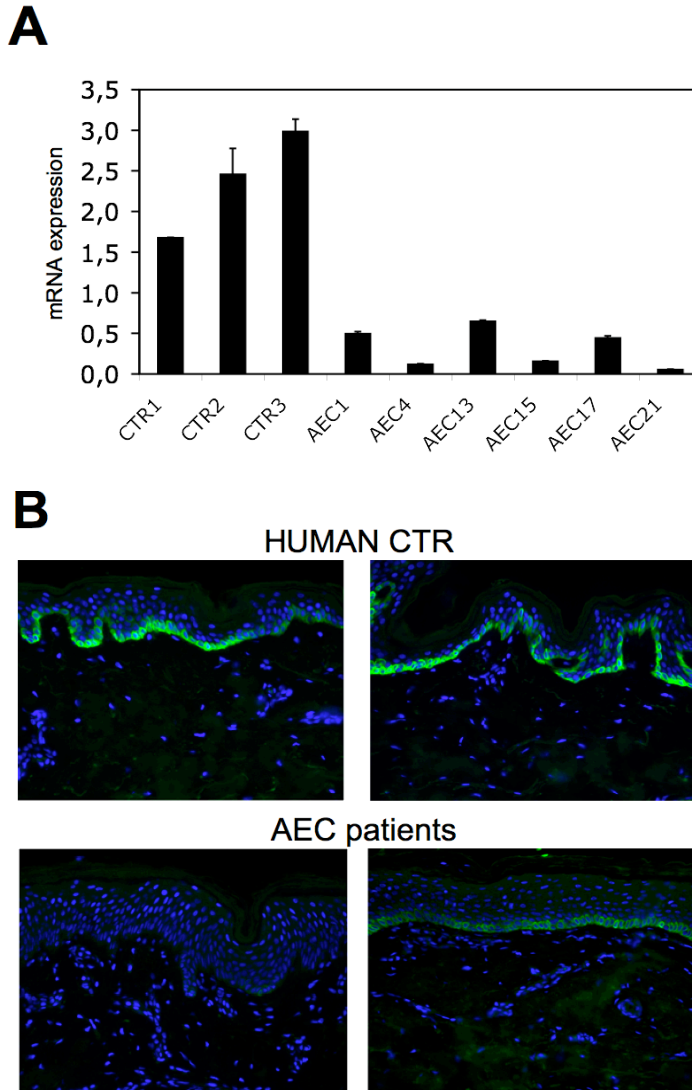


Figure 19. Krt15 is expressed at low levels in AEC patients. **A** Real time PCR analysis on mRNA from several AEC patients compared to several human controls (CTR). **B.** Immunofluorescence staining for krt15 in skin section of two different AEC patients compared to two human controls (CTR).

3.6 Skin hypoplasia is caused by increased apoptosis of basal cell compartment

p63 has been involved in apoptosis with variable outcomes depending on the p63 isoform taken into consideration (63-66). We evaluated if an increase in apoptosis could account for the hypoplastic phenotype of $p63^{+/L514F}$ mice. We found a significant difference in the epidermis of $p63^{+/L514F}$ versus wild-type mice at P0 stage (Fig.20). Staining for active caspase 3 was localized in the basal layer of mutant epidermis in which are putatively interspersed epidermal stem cells (Fig.20). This finding could account for the morphology of mutant colonies in the colony-assay (Fig.16C).

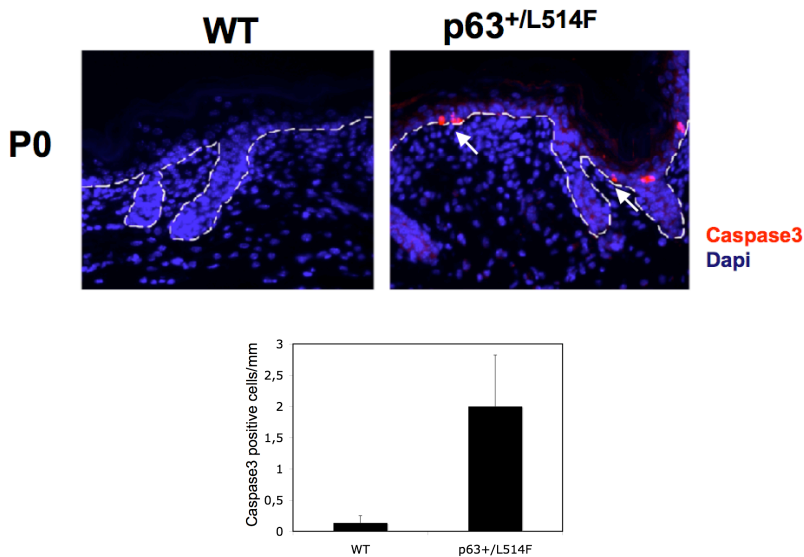


Figure 20. Caspase 3 is increased in the epidermis of $p63^{+/L514F}$ mice. Immunofluorescence staining on $p63^{+/L514F}$ versus wild-type back-skin section from mice at P0 stage with active caspase 3 antibody. Some basal cells in $p63^{+/L514F}$ epidermis are positive to active caspase 3 (white arrows). Below: quantification of caspase 3 positive cells for field (Original magnification 20X).

3.7 Loss or gain of function? Analysis of mutation in $p63^{L514F}$ mice

Mice with only one copy of p63 ($p63^{+/-}$) are indistinguishable from wild-type littermates because one copy is sufficient to maintain the ectodermal development in mice. The L514F missense mutation falls in the first α -helix of SAM domain and causes an autosomal dominant phenotype. To uncover if the effect of mutation is produced by a gain of function or by a dominant negative effect of the mutant isoform on the p63 tetramer, we mated chimeras carrying L514F mutant cells in their germ line with $p63^{+/-}$ mice to obtain $p63^{L514F}$ mice so that we could unmask the effect of the mutation on a p63 background in which only p63 isoforms that do not possess SAM domain are expressed (p63 β and γ) in single copy. $p63^{L514F}$ were born with cleft palate, craniofacial abnormalities and limb defects (Fig.21A). These abnormalities were more severe in $p63^{-/-}$ mice. We found that the epidermal phenotype of $p63^{L514F}$ mice was very similar to that of $p63^{-/-}$ mice (Fig.21B). The marker of basal layer Krt14 was expressed at E18.5 in both models in a discontinuous monolayer often detached from derma; the spinous, the granular and the corneous layers were absent in both models as showed by immunofluorescence staining with markers of stratified layers (data not shown). Thus, we showed that stratification did not occur in either $p63^{L514F}$ or $p63^{-/-}$ mice. This finding indicates that L514F mutation affects primarily epidermal development, and to a lesser extent limb and craniofacial development. Thus, an intact α isoform is essential for epidermal development, whereas γ and β isoforms can at least in part rescue limb and craniofacial defects.

A



B

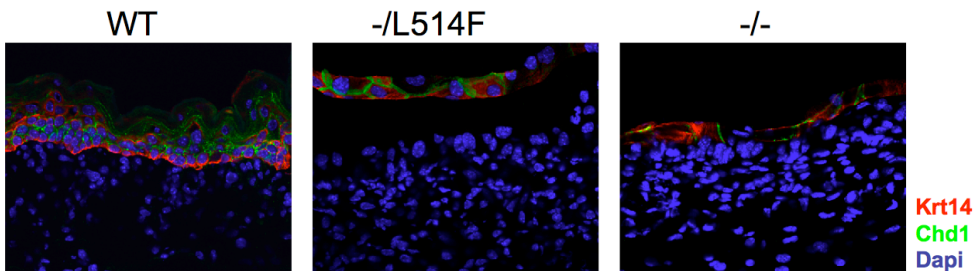


Figure 21. Comparison between $p63^{-/L514F}$ and $p63^{-/}$ mice. **A.** Sagittal views of E18.5 control, $p63^{-/}$ and $p63^{-/L514F}$ embryos. Both models have no eyelids, whisker pads, skin and related appendages, which are present on the wild-type control. $p63^{-/}$ embryos have more hypoplastic upper and lower jaws compared to $p63^{-/L514F}$ embryos. $p63^{-/}$ embryos lacks distal components of the forelimb and all component of hindlimbs while in the $p63^{-/L514F}$ embryos the defect is milder. **B.** Immunofluorescence staining of Krt14 and Chd1 show a discontinue monolayer often detached from the dermis.

3.8 Molecular pathways involved in the pathogenesis of AEC syndrome

One of the crucial information that would be required to fully understand the pathogenesis of AEC syndrome is the function of the SAM domain. Yeast two-hybrid screenings (Y2H) in which p63 was used as bait, reported that ABBP1, a splicing regulator, binds to the SAM domain (67). Physical association of p63 and ABBP1 induced alternative splicing of the Fgfr2 (fibroblast growth factor receptor 2) toward the Ksam isoform essential for epithelial differentiation. AEC mutations were reported to disrupt p63-ABBP1 association with a consequent decrease in Ksam isoform (67). To test the possibility that Fgfr2 may undergo differential splicing in *p63*^{+/*L514F*} mutant mice compared to wild-type, we performed a Real time PCR analysis on both mutant and wt mice. We did not observed any difference either in isoform of Fgfr2 Bek (the prevalent isoform in dermis) or in Ksam (Fig.22).

Results

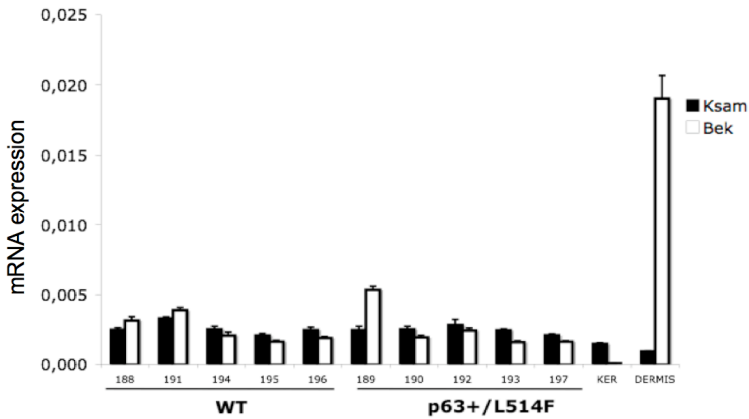


Figure 22. Expression of Fgfr2 isoforms in $p63^{+/L514F}$ mice . Ksam (black bars) and Fgfr2–Bek (white bars) splicing isoforms were measured at the mRNA level by real time RT–PCR in $p63^{+/L514F}$ and wild–type (WT) epidermis at P0 stage. As control these isoforms were measured in mouse primary keratinocytes (KER), where Ksam is the only isoform expressed, and in wild–type dermis were the prevalent isoform is Fgfr2–Bek as expected.

To uncover other possible pathways that may be at the basis of the hypoplastic skin phenotype, we considered changes in gene expression profile of $p63^{+/L514F}$ versus wild-type mice and tried to correlate the phenotype of these mice to those of other skin models.

Double knock-out mice for Mek1 and Mek2 display a similar hypoplastic phenotype due to loss of ERK1/2 phosphorylation (68). Thus, we measured levels of phosphorylated ERK1-2 by immunoblotting on keratinocytes isolated from $p63^{+/L514F}$ and wild-type mice under basal condition and after induction of MAPK pathway with insulin-like growth factor 2 (IGF2). No

Results

differences between wild-type and $p63^{+/L514F}$ keratinocytes could be detected (Fig 22A).

We performed immunoblotting analysis of phosphorylated ERK1-2 also on $p63^{+/L514F}$ and wild-type keratinocytes plated at low density and with a medium that favors the growth of epidermal stem cells (see Materials and Methods). We tested three different wild-type and mutant sets recovered after one week of culture. Also this subpopulation of cells that might be responsible for the epidermal phenotype of $p63^{+/L514F}$ mice, did not display differences in phosphorylation of ERK1-2 (Fig 22B).

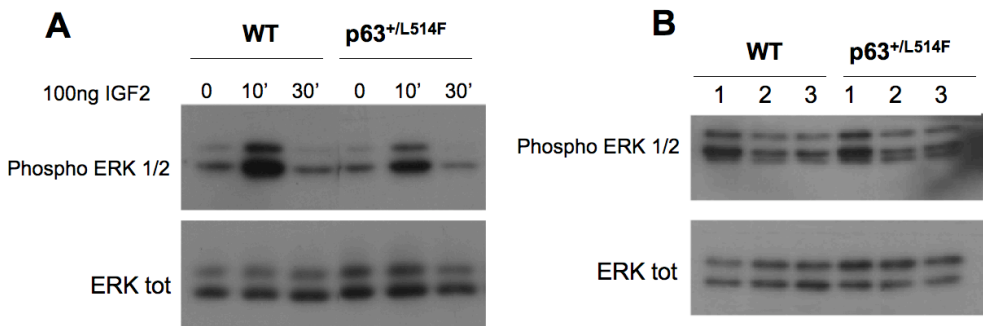


Figure 22. Levels of ERK phosphorylation in $p63^{+/L514F}$ and wild-type keratinocytes. **A.** Immunoblotting analysis of phosphorylated ERK1/2 on keratinocytes isolated from $p63^{+/L514F}$ and wild-type newborn mice. Cells were induced with 100ng of IGF2 at different time point (10', 30') or left untreated (0). **B.** Immunoblotting analysis of phosphorylated ERK1/2 on epidermal stem cells after one week of culture. We analyzed three different wild-type and mutant sets. Total ERK level was used as control.

Among the biochemical pathways that may be involved in maintenance of an appropriate stem cell compartment in skin, we tested the possibility that

Results

$p63^{+/L514F}$ expression may affect the insulin/IGF signaling. This signaling pathway is key regulator of energy metabolism and growth. We found that IGF2 is strongly reduced in gene chips analysis and we confirmed this result in $p63^{+/L514F}$ versus wild-type skin at mRNA and protein levels (Fig. 23A, B).

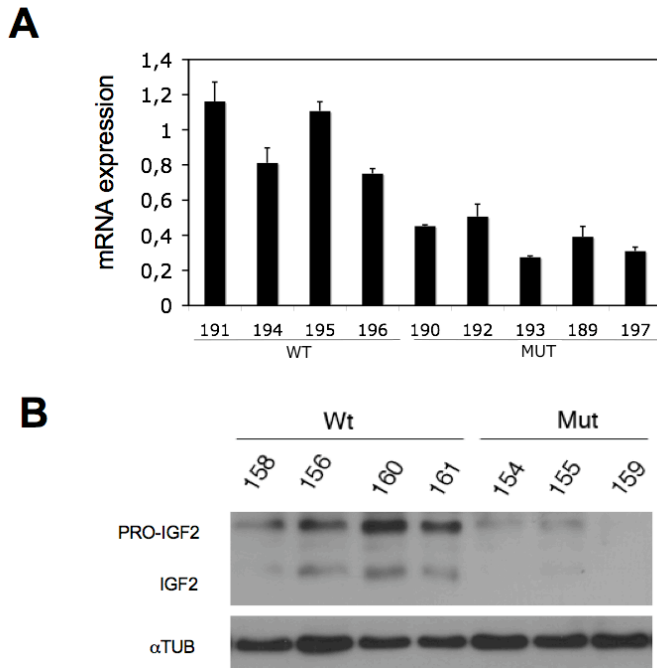


Figure 23. Expression of Igf2 in $p63^{+/L514F}$ mice epidermis. **A.** Real time PCR analysis of mRNA extracted from epidermis of mutant versus wild type mice using oligos that anneal on Igf2 gene. **B.** Immunoblotting analysis of mutant versus wild-type epidermal extracts using an antibody against the Igf2 protein.

Results

Interestingly, it has been recently reported that mice with an epidermal deletion of the Igf receptor 1 (Igfr1) have a very similar hypoplastic phenotype with no obvious proliferation or differentiation defects (69). Conversely, overexpression of Igf2 results in epidermal thickening and increased nuclear counts in the absence of an obvious increase in cell proliferation (70). The phenotype of Igfr1 null epidermis has been ascribed to a decreased proliferative potential of epidermal stem cells. Igfr1 null epidermis displays a strong reduction of Krt15 expression, and a defect in colony-forming assay. Similar reductions were observed in $p63^{+/L514F}$ mice (Fig. 16, 18) thus suggesting a strong overlap between the phenotypes of the two mouse models.

We evaluated the expression of Akt, a downstream kinase of IR/IGF-1R signaling pathway, under basal condition and after induction of PI3K-Akt pathway by treatment with IGF2. Similarly to what previously observed in mice with epidermal deletion of Igfr1, Akt phosphorylation remained at physiological levels in $p63^{+/L514F}$ mice. However, as in mice with epidermal deletion of Igfr1, total levels of Akt were higher in $p63^{+/L514F}$ mice than in their wild-type littermates, suggesting a compensatory mechanism.

Results

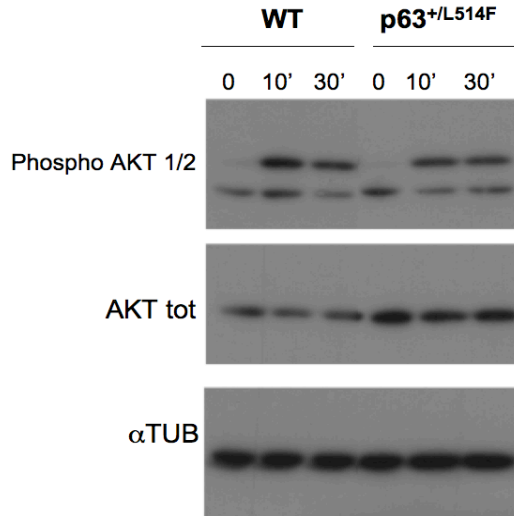


Figure 22. Levels of Akt phosphorylation in p63^{+/L514F} and wild-type keratinocytes.A. Immunoblotting analysis of phosphorylated AKT on keratinocytes isolated from p63^{+/L514F} and wild-type newborn mice. Cells were induced with 100ng of IGF2 at different time point (10', 30') or left untreated (0). α-TUBULIN (αTUB) was used to normalize samples.

4. DISCUSSION

$p63^{+/L514F}$ mice constitute the first mouse model generated to study the pathogenesis of AEC syndrome. This model carries a clinically relevant point mutation in the SAM domain of the p63 alpha isoform, and faithfully recapitulates the human disorder.

In the characterization of the AEC mouse model, we essentially focused our attention on skin defects for their severity in AEC patients and for the dramatic epidermal phenotype observed in p63 null mice. We find that the epithelial phenotype of $p63^{L514F/+}$ mice is characterized by severe hypoplasia of epidermis and hair follicle. Our working hypothesis is that this epidermal hypoplasia results in the skin fragility observed in AEC mice and in patients. Our results indicate that skin of $p63^{+/L514F}$ is hypoplastic in spite of a normal proliferation and differentiation. During this study we collected evidence suggesting that the skin phenotype is caused by a defect in the proliferative potential and/or survival of epidermal progenitor cells. This defect is associated with an increased apoptosis of the basal compartment of epidermis.

Hypoplastic phenotype in previously described mouse models has been ascribed to either defective proliferation or differentiation. In particular, $Fgfr2-IIIb^{-/-}$ mice and $Fgf10^{-/-}$ mice are characterized by a severe skin hypoplasia, associated with cell proliferation defect (71, 72). Similarly, disruption of the MEK/ERK pathway results in skin hypoplasia and reduced cell growth (68, 73). Since p63 has an important role in epidermal proliferation (53, 54) we asked if a reduced proliferative potential of

Discussion

epidermal cells could explain the reduced skin thickness. However cell proliferation in the basal compartment of the epidermis and hair follicle of $p63^{+/L514F}$ mice was unaffected either at different stages of skin maturation (E13.5, E16.5, and P0) or in cultured primary keratinocytes. In addition we found that expression of *Fgfr2* isoforms and ERK phosphorylation were unaffected in $p63^{+/L514F}$ mutant mice.

Hypoplasia could also be ascribed to a defective differentiation (74). p63 was identified as a crucial positive regulator of epidermal stratification (17, 55). In our mouse model differentiation occurs normally as showed by the correct localization and expression of differentiation markers like Krt1 and Krt10, Involucrin, Loricrin, and as confirmed by the permeability assay that demonstrate the presence of a complete skin barrier. These findings are not in contrast with a role of p63 in differentiation, rather suggest that only a subset of p63 functions are altered by the L514F heterozygous mutation.

We collected evidence in support of an involvement of p63 in maintenance of the epidermal stem cell compartment. The first evidence is constitute by the severe epithelial phenotype of p63 null mice that has been interpreted to result from both lack of commitment of the immature ectoderm to the epidermal lineage (17), and to a defect in the proliferative potential of the p63-deficient epidermal progenitor cells (18). In addition, p63 is expressed in holoclones (colonies generated by stem cells) of human keratinocytes and corneal cells (75, 76). To investigate the possible mechanism of action of p63 in maintaining proliferative potential of epithelial stem cells, Senoo et al focused their attention on thymus development of $p63^{-/-}$ mice since in this mouse model the epidermis is absent. They showed that the deletion of p63 is responsible for thymus hypoplasia without affecting differentiation or

commitment of epithelial stem cells. By clonogenic analysis performed on cultured thymus epithelial cells, they demonstrated that p63-null colonies have a reduced number of cells compared to wild-type colonies associated to an increase in the rate of apoptosis of thymic epithelial cells *in vivo* (57). In agreement with studies on thymic epithelial cells, clonogenic analysis performed on rat epidermal keratinocytes transfected with an shRNA against p63 demonstrated that p63-deficient colonies are smaller than their wild-type counterpart (57).

We show here that in $p63^{+/L514F}$ mice, commitment of all epidermal lineages occurs properly, whereas proliferative potential/survival of epidermal stem cells is defective. We estimated the number of epidermal stem cells by performing FACS analysis with the cell surface markers CD49f and CD71, on freshly isolated keratinocyte. Cells identified as CD49f^{bri}/CD71^{dim} are putative epidermal stem cells (see Introduction). We found that this cell population is strongly reduced in $p63^{+/L514F}$ mice epidermis versus wild-type. In addition, colony-forming assay showed that colonies derived from $p63^{+/L514F}$ keratinocytes have a reduced size and a different morphology compared to wild-type. Finally, we showed that both mRNA and protein levels of the putative skin stem cell marker Krt15 are strongly reduced in $p63^{+/L514F}$ mice compared to wild-type. Interestingly we found a reduction of both at mRNA and protein levels of Krt15 in several AEC patients affected by different mutations. Thus our findings indicate that L514F heterozygous mutation does not affect epidermal stratification or proliferation, whereas it specifically affects stem cell compartment.

Our data indicate that the defect in stem cell compartment is due to an increased rate of apoptosis in the basal layer of epidermis of newborn

Discussion

$p63^{+/L514F}$ compared to wild-type mice. A role of p63 in apoptosis was previously suggested (63-66). Rocco et al. showed that $\Delta Np63\alpha$ act as a survival factor by inhibiting p73-dependent apoptosis (77-79). Future work will be required to assess whether apoptotic cells that we have detected in the basal layer of the mutant epidermis, belong to the pool of progenitor cells.

In the attempt to uncover the molecular basis of AEC syndrome we hypothesize two alternative biological mechanism. Strong evidence suggests that the Igf receptor 1 (Igfr1) signaling pathway could be affected in AEC mice. It was demonstrated that IGF2, a ligand of Igfr1, is implicated in proliferative potential of human embryonic stem cells (80) and that its overexpression results in epidermal thickening and increased nuclear counts (70). Our microarray data indicate that $p63^{+/L514F}$ have reduced level of Igf2. These data were confirmed both at mRNA and protein levels.

In addition, mice with epidermal deletion of *Igfr1* have a very similar hypoplastic phenotype to $p63^{+/L514F}$ mice with no obvious proliferation or differentiation defects (69). Igfr1 null epidermis displays a strong reduction of Krt15 protein levels and a defect in colony-forming assay. Thus both the skin phenotypes of mice with epidermal deletion of *Igfr1* and $p63^{+/L514F}$ mice were caused by a decreased proliferative potential of epidermal stem cells. Taken together these data suggest that mutations in the SAM domain may cause a defect in Igf2/Igfr1 signaling pathway, resulting in reduced stem cell proliferation potential and cell survival.

An alternative possibility could involve the ability of $\Delta Np63\alpha$ to interfere with p73-mediated apoptosis. The p63 and p73 proteins contain a highly homologous oligomerization domain (>60% identical) and are able to

heterodimerize (65). Δ Np63 α was shown to inhibit p73-dependent transactivation both by an “off –promoter” mechanism involving sequestration of p73 protein and by binding to the promoter of the proapoptotic gene *Puma* suppressing its transcription (65). Thus, we postulate that in $p63^{+/L514F}$ mice heterodimerization between p63 and p73 may be defective and p73 protein may be free to activate an apoptotic program in the basal compartment. Future experiment will be required to test this hypothesis on keratinocytes isolated either from wild-type or $p63^{+/L514F}$ mice.

A search for interactors of the SAM domain has been performed by several laboratories, including ours. However, we have not been able to identify protein interacting with this domain. A distinct possibility is that SAM domain may be crucial for the formation of specific transcriptional complexes, involved in regulation of a subset of targets. Thus, typical developmental defects of AEC syndrome could be caused by disruption of these interactions rather than by alteration of direct p63 transcriptional targets. This hypothesis is supported by our microarray analysis indicating that only a subset of p63 target genes is affected by the mutation.

In the absence of its wild-type counterpart, the L514F mutant allele causes a similar epithelial defect of the one observed in $p63^{-/-}$ mice suggesting that epidermal defects observed in our AEC mouse model could be attributed to a dominant-negative effect rather than a gain-of-function. Such dominant-negative effect could act on a subset of specific functions regulated by the SAM domain. Facial and limb malformation are less severe in $p63^{-/L514F}$ than in $p63^{-/-}$, whereas the severe epidermal defect is identical in the two mouse model. Taken together these data suggest that the p63 β and p63 γ

Discussion

isoforms present in a single copy in the $p63^{-/L514F}$ mice, can partially rescue the limb and facial phenotype, while are unable to rescue the epidermal phenotype. Thus we showed that the SAM domain plays a crucial role in epidermal morphogenesis since $p63^{+/L514F}$ keratinocytes, in presence of an intact DNA binding domain, show a deficit in the epidermal progenitor cell compartment.

In conclusion, our mouse model will be useful for us and more in general for the scientific community engaged in this field to understand the pathogenesis of this complex disorder, characterize more in detail identity and property of epidermal stem cells and to set up clinically relevant treatments to alleviate skin symptoms in AEC children.

REFERENCES

1. Rook A & Burns T (2004) *Rook's textbook of dermatology* (Blackwell Science, Malden, Mass.) 7th Ed p 4 v. (paged continuously).
2. Potten CS, Kovacs L, & Hamilton E (1974) Continuous labelling studies on mouse skin and intestine. *Cell Tissue Kinet* 7(3):271-283.
3. Potten CS & Morris RJ (1988) Epithelial stem cells in vivo. *J Cell Sci Suppl* 10:45-62.
4. Potten CS (1974) The epidermal proliferative unit: the possible role of the central basal cell. *Cell Tissue Kinet* 7(1):77-88.
5. Clayton E, *et al.* (2007) A single type of progenitor cell maintains normal epidermis. *Nature* 446(7132):185-189.
6. Adams JC & Watt FM (1991) Expression of beta 1, beta 3, beta 4, and beta 5 integrins by human epidermal keratinocytes and non-differentiating keratinocytes. *J Cell Biol* 115(3):829-841.
7. Tani H, Morris RJ, & Kaur P (2000) Enrichment for murine keratinocyte stem cells based on cell surface phenotype. *Proc Natl Acad Sci USA* 97(20):10960-10965.
8. Osada M, *et al.* (1998) Cloning and functional analysis of human p51, which structurally and functionally resembles p53. *Nat Med* 4(7):839-843.
9. Oshima H, Rochat A, Kedzia C, Kobayashi K, & Barrandon Y (2001) Morphogenesis and renewal of hair follicles from adult multipotent stem cells. *Cell* 104(2):233-245.
10. Schmale H & Bamberger C (1997) A novel protein with strong homology to the tumor suppressor p53. *Oncogene* 15(11):1363-1367.
11. Trink B, *et al.* (1998) A new human p53 homologue. *Nat Med* 4(7):747-748.
12. Yang A, *et al.* (1998) p63, a p53 homolog at 3q27-29, encodes multiple products with transactivating, death-inducing, and dominant-negative activities. *Mol Cell* 2(3):305-316.
13. Dohn M, Zhang S, & Chen X (2001) p63alpha and DeltaNp63alpha can induce cell cycle arrest and apoptosis and differentially regulate p53 target genes. *Oncogene* 20(25):3193-3205.
14. Helton ES, Zhu J, & Chen X (2006) The unique NH2-terminally deleted (DeltaN) residues, the PXXP motif, and the PPXY motif are

References

- required for the transcriptional activity of the DeltaN variant of p63. *J Biol Chem* 281(5):2533-2542.
15. Serber Z, *et al.* (2002) A C-terminal inhibitory domain controls the activity of p63 by an intramolecular mechanism. *Mol Cell Biol* 22(24):8601-8611.
 16. Kemp CJ, Wheldon T, & Balmain A (1994) p53-deficient mice are extremely susceptible to radiation-induced tumorigenesis. *Nat Genet* 8(1):66-69.
 17. Mills AA, *et al.* (1999) p63 is a p53 homologue required for limb and epidermal morphogenesis. *Nature* 398(6729):708-713.
 18. Yang A, *et al.* (1999) p63 is essential for regenerative proliferation in limb, craniofacial and epithelial development. *Nature* 398(6729):714-718.
 19. Yang A, *et al.* (2000) p73-deficient mice have neurological, pheromonal and inflammatory defects but lack spontaneous tumours. *Nature* 404(6773):99-103.
 20. Sanford LP, *et al.* (1997) TGFbeta2 knockout mice have multiple developmental defects that are non-overlapping with other TGFbeta knockout phenotypes. *Development* 124(13):2659-2670.
 21. Mo R, *et al.* (1997) Specific and redundant functions of Gli2 and Gli3 zinc finger genes in skeletal patterning and development. *Development* 124(1):113-123.
 22. Thomason HA, Dixon MJ, & Dixon J (2008) Facial clefting in Tp63 deficient mice results from altered Bmp4, Fgf8 and Shh signaling. *Dev Biol* 321(1):273-282.
 23. Celli J, *et al.* (1999) Heterozygous germline mutations in the p53 homolog p63 are the cause of EEC syndrome. *Cell* 99(2):143-153.
 24. van Bokhoven H, *et al.* (1999) Limb mammary syndrome: a new genetic disorder with mammary hypoplasia, ectrodactyly, and other Hand/Foot anomalies maps to human chromosome 3q27. *Am J Hum Genet* 64(2):538-546.
 25. Rinne T, Brunner HG, & van Bokhoven H (2007) p63-associated disorders. *Cell Cycle* 6(3):262-268.
 26. van Bokhoven H & Brunner HG (2002) Splitting p63. *Am J Hum Genet* 71(1):1-13.
 27. Bertola DR, *et al.* (2004) Molecular evidence that AEC syndrome and Rapp-Hodgkin syndrome are variable expression of a single genetic disorder. *Clin Genet* 66(1):79-80.

References

28. McGrath JA, *et al.* (2001) Hay-Wells syndrome is caused by heterozygous missense mutations in the SAM domain of p63. *Hum Mol Genet* 10(3):221-229.
29. Rinne T, Hamel B, van Bokhoven H, & Brunner HG (2006) Pattern of p63 mutations and their phenotypes--update. *Am J Med Genet A* 140(13):1396-1406.
30. Brunner HG, Hamel BC, & Van Bokhoven H (2002) The p63 gene in EEC and other syndromes. *J Med Genet* 39(6):377-381.
31. Hay RJ & Wells RS (1976) The syndrome of ankyloblepharon, ectodermal defects and cleft lip and palate: an autosomal dominant condition. *Br J Dermatol* 94(3):277-289.
32. Tsutsui K, *et al.* (2003) A novel p63 sterile alpha motif (SAM) domain mutation in a Japanese patient with ankyloblepharon, ectodermal defects and cleft lip and palate (AEC) syndrome without ankyloblepharon. *Br J Dermatol* 149(2):395-399.
33. Rinne T, *et al.* (2008) A novel translation re-initiation mechanism for the p63 gene revealed by amino-terminal truncating mutations in Rapp-Hodgkin/Hay-Wells-like syndromes. *Hum Mol Genet* 17(13):1968-1977.
34. Qiao F & Bowie JU (2005) The many faces of SAM. *Sci STKE* 2005(286):re7.
35. Kim CA & Bowie JU (2003) SAM domains: uniform structure, diversity of function. *Trends Biochem Sci* 28(12):625-628.
36. Bocconi P, MacGrogan D, Scandura JM, & Nimer SD (2003) The human L(3)MBT polycomb group protein is a transcriptional repressor and interacts physically and functionally with TEL (ETV6). *J Biol Chem* 278(17):15412-15420.
37. Thanos CD & Bowie JU (1999) p53 Family members p63 and p73 are SAM domain-containing proteins. *Protein Sci* 8(8):1708-1710.
38. Schultz J, Ponting CP, Hofmann K, & Bork P (1997) SAM as a protein interaction domain involved in developmental regulation. *Protein Sci* 6(1):249-253.
39. Thanos CD, Goodwill KE, & Bowie JU (1999) Oligomeric structure of the human EphB2 receptor SAM domain. *Science* 283(5403):833-836.
40. Stapleton D, Balan I, Pawson T, & Sicheri F (1999) The crystal structure of an Eph receptor SAM domain reveals a mechanism for modular dimerization. *Nat Struct Biol* 6(1):44-49.

References

41. Cicero DO, *et al.* (2006) NMR structure of the p63 SAM domain and dynamical properties of G534V and T537P pathological mutants, identified in the AEC syndrome. *Cell Biochem Biophys* 44(3):475-489.
42. Liu P, Jenkins NA, & Copeland NG (2003) A highly efficient recombineering-based method for generating conditional knockout mutations. *Genome Res* 13(3):476-484.
43. Hardman MJ, Sisi P, Banbury DN, & Byrne C (1998) Patterned acquisition of skin barrier function during development. *Development* 125(8):1541-1552.
44. Wang Z, Wong P, Langbein L, Schweizer J, & Coulombe PA (2003) Type II epithelial keratin 6hf (K6hf) is expressed in the companion layer, matrix, and medulla in anagen-stage hair follicles. *J Invest Dermatol* 121(6):1276-1282.
45. Wong P & Coulombe PA (2003) Loss of keratin 6 (K6) proteins reveals a function for intermediate filaments during wound repair. *J Cell Biol* 163(2):327-337.
46. Paladini RD, Takahashi K, Bravo NS, & Coulombe PA (1996) Onset of re-epithelialization after skin injury correlates with a reorganization of keratin filaments in wound edge keratinocytes: defining a potential role for keratin 16. *J Cell Biol* 132(3):381-397.
47. Della Gatta G, *et al.* (2008) Direct targets of the TRP63 transcription factor revealed by a combination of gene expression profiling and reverse engineering. *Genome Res* 18(6):939-948.
48. Yang A, *et al.* (2006) Relationships between p63 binding, DNA sequence, transcription activity, and biological function in human cells. *Mol Cell* 24(4):593-602.
49. Ihrie RA, *et al.* (2005) Perp is a p63-regulated gene essential for epithelial integrity. *Cell* 120(6):843-856.
50. Romano RA, Birkaya B, & Sinha S (2007) A functional enhancer of keratin14 is a direct transcriptional target of deltaNp63. *J Invest Dermatol* 127(5):1175-1186.
51. Ellisen LW, *et al.* (2002) REDD1, a developmentally regulated transcriptional target of p63 and p53, links p63 to regulation of reactive oxygen species. *Mol Cell* 10(5):995-1005.
52. Rogers MA, *et al.* (2005) Characterization of new members of the human type II keratin gene family and a general evaluation of the keratin gene domain on chromosome 12q13.13. *J Invest Dermatol* 124(3):536-544.

References

53. Lee H & Kimelman D (2002) A dominant-negative form of p63 is required for epidermal proliferation in zebrafish. *Dev Cell* 2(5):607-616.
54. Truong AB, Kretz M, Ridky TW, Kimmel R, & Khavari PA (2006) p63 regulates proliferation and differentiation of developmentally mature keratinocytes. *Genes Dev* 20(22):3185-3197.
55. Koster MI, Kim S, Mills AA, DeMayo FJ, & Roop DR (2004) p63 is the molecular switch for initiation of an epithelial stratification program. *Genes Dev* 18(2):126-131.
56. Nguyen BC, *et al.* (2006) Cross-regulation between Notch and p63 in keratinocyte commitment to differentiation. *Genes Dev* 20(8):1028-1042.
57. Senoo M, Pinto F, Crum CP, & McKeon F (2007) p63 Is essential for the proliferative potential of stem cells in stratified epithelia. *Cell* 129(3):523-536.
58. Redvers RP, Li A, & Kaur P (2006) Side population in adult murine epidermis exhibits phenotypic and functional characteristics of keratinocyte stem cells. *Proc Natl Acad Sci U S A* 103(35):13168-13173.
59. Strachan LR, Scalapino KJ, Lawrence HJ, & Ghadially R (2008) Rapid adhesion to collagen isolates murine keratinocytes with limited long-term repopulating ability in vivo despite high clonogenicity in vitro. *Stem Cells* 26(1):235-243.
60. Li A, Pouliot N, Redvers R, & Kaur P (2004) Extensive tissue-regenerative capacity of neonatal human keratinocyte stem cells and their progeny. *J Clin Invest* 113(3):390-400.
61. Webb A, Li A, & Kaur P (2004) Location and phenotype of human adult keratinocyte stem cells of the skin. *Differentiation* 72(8):387-395.
62. Liu Y, Lyle S, Yang Z, & Cotsarelis G (2003) Keratin 15 promoter targets putative epithelial stem cells in the hair follicle bulge. *J Invest Dermatol* 121(5):963-968.
63. Flores ER, *et al.* (2002) p63 and p73 are required for p53-dependent apoptosis in response to DNA damage. *Nature* 416(6880):560-564.
64. Liefer KM, *et al.* (2000) Down-regulation of p63 is required for epidermal UV-B-induced apoptosis. *Cancer Res* 60(15):4016-4020.
65. Rocco JW, Leong CO, Kuperwasser N, DeYoung MP, & Ellisen LW (2006) p63 mediates survival in squamous cell carcinoma by suppression of p73-dependent apoptosis. *Cancer Cell* 9(1):45-56.

References

66. Sayan BS, *et al.* (2007) Cleavage of the transactivation-inhibitory domain of p63 by caspases enhances apoptosis. *Proc Natl Acad Sci U S A* 104(26):10871-10876.
67. Fomenkov A, *et al.* (2003) P63 alpha mutations lead to aberrant splicing of keratinocyte growth factor receptor in the Hay-Wells syndrome. *J Biol Chem* 278(26):23906-23914.
68. Scholl FA, *et al.* (2007) Mek1/2 MAPK kinases are essential for Mammalian development, homeostasis, and Raf-induced hyperplasia. *Dev Cell* 12(4):615-629.
69. Stachelscheid H, *et al.* (2008) Epidermal insulin/IGF-1 signalling control interfollicular morphogenesis and proliferative potential through Rac activation. *EMBO J* 27(15):2091-2101.
70. Bennett WR, Crew TE, Slack JM, & Ward A (2003) Structural-proliferative units and organ growth: effects of insulin-like growth factor 2 on the growth of colon and skin. *Development* 130(6):1079-1088.
71. Revest JM, *et al.* (2001) Fibroblast growth factor receptor 2-IIIb acts upstream of Shh and Fgf4 and is required for limb bud maintenance but not for the induction of Fgf8, Fgf10, Msx1, or Bmp4. *Dev Biol* 231(1):47-62.
72. Min H, *et al.* (1998) Fgf-10 is required for both limb and lung development and exhibits striking functional similarity to Drosophila branchless. *Genes Dev* 12(20):3156-3161.
73. Dumesic PA, Scholl FA, Barragan DI, & Khavari PA (2009) Erk1/2 MAP kinases are required for epidermal G2/M progression. *J Cell Biol* 185(3):409-422.
74. Suzuki K, *et al.* (2000) Defective terminal differentiation and hypoplasia of the epidermis in mice lacking the Fgf10 gene. *FEBS Lett* 481(1):53-56.
75. Parsa R, Yang A, McKeon F, & Green H (1999) Association of p63 with proliferative potential in normal and neoplastic human keratinocytes. *J Invest Dermatol* 113(6):1099-1105.
76. Pellegrini G, *et al.* (2001) p63 identifies keratinocyte stem cells. *Proc Natl Acad Sci U S A* 98(6):3156-3161.
77. Gong JG, *et al.* (1999) The tyrosine kinase c-Abl regulates p73 in apoptotic response to cisplatin-induced DNA damage. *Nature* 399(6738):806-809.
78. Irwin MS, *et al.* (2003) Chemosensitivity linked to p73 function. *Cancer Cell* 3(4):403-410.

References

79. Urist M, Tanaka T, Poyurovsky MV, & Prives C (2004) p73 induction after DNA damage is regulated by checkpoint kinases Chk1 and Chk2. *Genes Dev* 18(24):3041-3054.
80. Bendall SC, *et al.* (2007) IGF and FGF cooperatively establish the regulatory stem cell niche of pluripotent human cells in vitro. *Nature* 448(7157):1015-1021.

References
